Published in final edited form as:

Circ Res. 2020 September 25; 127(8): 997–1022. doi:10.1161/CIRCRESAHA.120.317295.

Parallel Murine and Human Plaque Proteomics Reveals Pathways of Plaque Rupture

Tomáš Vaisar[1,*], **Jie H. Hu**[1,*], **Nathan Airhart**[1], **Kate Fox**[1], **Jay Heinecke**[1], **Roberto F. Nicosia**[2,4], **Ted Kohler**[3,4], **Zachary E. Potter**[5], **Gabriel M. Simon**[6], **Melissa M. Dix**[5], **Benjamin F. Cravatt**[5], **Sina A. Gharib**[1,*], **David A. Dichek**[1,*]

[1]Department of Medicine, University of Washington, Seattle, WA;

[2]Department of Pathology and Laboratory Medicine, University of Washington, Seattle, WA;

[3]Department of Surgery (T.K.), University of Washington, Seattle, WA;

[4]Surgery and Pathology and Laboratory Medicine, VA Puget Sound Health Care System, the Department of Chemistry,

[5]The Scripps Research Institute, La Jolla, CA,

[6]Vividion Therapeutics

Abstract

Rationale: Plaque rupture is the proximate cause of most myocardial infarctions and many strokes. However, the molecular mechanisms that precipitate plaque rupture are unknown.

Objective: By applying proteomic and bioinformatic approaches in mouse models of protease-induced plaque rupture and in ruptured human plaques, we aimed to illuminate biochemical pathways through which proteolysis causes plaque rupture and identify substrates that are cleaved in ruptured plaques.

Methods and Results: We performed shotgun proteomics analyses of aortas of transgenic mice with macrophage-specific overexpression of urokinase (SR-uPA$^{+/0}$ mice) and of SR-uPA$^{+/0}$ bone-marrow transplant recipients and we used bioinformatic tools to evaluate protein abundance and functional-category enrichment in these aortas. In parallel, we performed shotgun proteomics and bioinformatics studies on extracts of ruptured and stable areas of freshly harvested human carotid plaques. We also applied a separate protein-analysis method (PROTOMAP) to attempt to identify substrates and proteolytic fragments in mouse and human plaque extracts. Approximately 10% of extracted aortic proteins were reproducibly altered in SR-uPA$^{+/0}$ aortas. Proteases, inflammatory-

Address correspondence to: Dr. David A. Dichek, Division of Cardiology, Department of Medicine, University of Washington School of Medicine, 1959 NE Pacific St Box 357710, Seattle, WA 98195-7710, ddichek@uw.edu.
*These authors contributed equally to this article

DISCLOSURES
None

SUPPLEMENTAL MATERIALS
Major Resources Table
Online Figures I – VI
Online Tables I – III
Online Data Sets I – XV

signaling molecules, as well as proteins involved with cell adhesion, the cytoskeleton, and apoptosis were increased. Extracellular-matrix proteins, including basement-membrane proteins, were decreased. Approximately 40% of proteins were altered in ruptured versus stable areas of human carotid plaques, including many of the same functional categories that were altered in SR-uPA$^{+/0}$ aortas. Collagens were minimally altered in SR-uPA$^{+/0}$ aortas and ruptured human plaques; however, several basement-membrane proteins were reduced in both SR-uPA$^{+/0}$ aortas and ruptured human plaques. PROTOMAP did not detect robust increases in proteolytic fragments of extracellular-matrix proteins in either setting.

Conclusions: Parallel studies of SR-uPA$^{+/0}$ mouse aortas and human plaques identify mechanisms that connect proteolysis with plaque rupture, including: inflammation, basement-membrane protein loss, and apoptosis. Basement-membrane protein loss is a prominent feature of ruptured human plaques, suggesting a major role for basement-membrane proteins in maintaining plaque stability.

Graphical Abstract

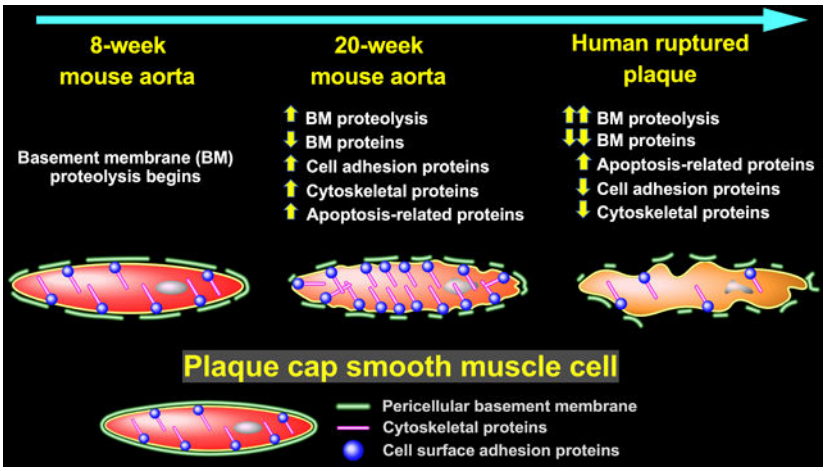

Keywords

Animal model (cardiovascular disease); basement membrane; extracellular matrix; carotid endarterectomy; proteomics; plaque rupture

Subject Terms:

Animal Models of Human Disease; Atherosclerosis; Cerebrovascular disease/Stroke; Proteomics; Vascular Biology

INTRODUCTION

Human atherosclerosis is usually an indolent disease, and can be asymptomatic for decades.[1] However, coronary and cerebral atherosclerosis can become unstable, precipitating angina, myocardial infarction, transient ischemic attacks, strokes, and death.[2, 3] The most common cause of instability of both coronary and cerebral atherosclerosis is “plaque rupture,” the physical disruption of an atherosclerotic plaque that exposes thrombogenic plaque contents,

leading to luminal thrombosis, thromboembolism, and vessel occlusion.[2, 4] Despite the importance of plaque rupture as the proximate cause of major adverse cardiovascular events, the molecular mechanisms that cause plaque rupture remain poorly understood. A better understanding of these mechanisms could facilitate recognition of rupture-prone plaques and hasten the development of therapies that prevent plaque rupture, thereby reducing myocardial infarctions, strokes, and cardiovascular deaths.

Proposed causes of plaque rupture include hemodynamic forces,[5, 6] plaque-cell apoptosis or senescence,[7–9] abnormal plaque microvasculature,[10] endoplasmic reticulum stress,[11] plaque microcalcifications,[12] inflammatory cytokines that alter plaque extracellular matrix (ECM) metabolism,[13] and increased vascular protease activity.[9, 13–15] Increased protease activity has received significant attention as a cause of plaque rupture, with candidate proteases including cathepsins, serine proteases, and matrix metalloproteinases (MMPs).[16] A role for proteases in plaque rupture is supported by detection of both increased protease activity and increased collagen cleavage in advanced human plaques.[17, 18] Preclinical data that support a role for proteases in plaque rupture include studies in which MMP deficiency or inhibition in mice increased plaque collagen content (interpreted as an indication of plaque stability),[19–21] and a study in which overexpression of constitutively active MMP9 in vascular wall cells of atherosclerotic mice produced histologic features that are shared with ruptured human plaques.[22] However, these studies have not produced a consensus that plaque rupture is caused primarily by proteolysis,[23] and the pathways that connect plaque proteolysis with plaque rupture remain hypothetical.[24] Identification of these pathways could provide new drug targets and could also reveal markers of unstable atherosclerosis.[25, 26]

To further investigate a role for proteases in plaque rupture, we have developed a transgenic mouse model in which the human scavenger receptor promoter drives macrophage-specific overexpression of the mouse urokinase-type plasminogen activator (PLAU) gene.[27] These "SR-uPA$^{+/0}$" mice have accelerated atherosclerosis; however, they die suddenly between 10 and 30 weeks of age, before developing a plaque-rupture phenotype. We overcame this obstacle by transplanting bone marrow from SR-uPA$^{+/0}$ *Apoe*$^{-/-}$ donors into 35-week-old nontransgenic *Apoe*$^{-/-}$ recipients (that already have rupture-prone innominate artery lesions).[28] Innominate artery lesions in SR-uPA$^{+/0}$ bone marrow transplant (BMT) recipients have an increased prevalence of histologic features of plaque rupture, including frequent intraplaque hemorrhage (61%) and fibrous cap disruption (78%). Moreover, aortas of SR-uPA$^{+/0}$ BMT recipients have significantly elevated MMP activity.[29]

Because the SR-uPA$^{+/0}$ mouse model convincingly connects increased artery wall protease activity with histologic features of plaque rupture, we hypothesized that atherosclerotic arteries of SR-uPA$^{+/0}$ mice and of recipients of SR-uPA$^{+/0}$ BMT would be informative experimental settings for: 1) unbiased proteomic studies aimed at elucidating the pathways through which elevated vascular protease activity causes plaque rupture; and 2) identifying specific protein or peptide markers of plaque rupture caused by elevated vascular protease activity. Accordingly, we performed proteomic analyses of aortas of SR-uPA$^{+/0}$ mice and of SR-uPA$^{+/0}$ BMT recipients and we applied bioinformatics tools to identify protein networks that are altered by increased aortic protease activity and could plausibly connect

increased protease activity with plaque rupture. To help accomplish these goals, we also analyzed extracts of atherosclerotic aortas of SR-uPA$^{+/0}$ BMT recipients with PROTOMAP, a proteomic analysis methodology designed to identify proteolytic events and peptide fragments in complex mixtures of proteins.[30] To explore the clinical relevance of findings from this mouse model, further test its validity as a model of human plaque rupture, and gain insights into mechanisms of human plaque rupture, we also carried out shotgun proteomics, bioinformatics analyses, and PROTOMAP studies on extracts of ruptured and stable areas of freshly harvested human carotid atherosclerotic plaques (using both discovery and validation cohorts) and we compared our results to those obtained from the SR-uPA$^{+/0}$ mouse. Our results show that basement-membrane protein loss is a reproducible finding in ruptured human plaques and is also a prominent feature of the SR-uPA$^{+/0}$ mouse plaque-rupture model.

METHODS

The data that support the findings of this study are available from the corresponding author on reasonable request. This study does not involve testing of a therapeutic or diagnostic agent in animal models. Please see the Major Resources Table in the Supplemental Materials.

Animal studies.

To begin development of tissue protein extraction techniques for enrichment of ECM proteins, aortic segments were obtained post-mortem from a chow-fed rabbit that was euthanized in the course of unrelated experiments.[31] All other animal experiments were performed with mice. All mice were *Apoe*$^{-/-}$ and were progeny of at least 10 generations of C57BL/6 backcrosses. Mice with macrophage-specific overexpression of urokinase-type plasminogen activator (SR-uPA$^{+/0}$ mice) were progeny of mice generated in our laboratory.[27] These mice are hemizygous for a transgene that includes the murine *Plau* gene driven by the human scavenger receptor promoter. SR-uPA$^{+/0}$ mice were bred with non-transgenic mice (SR-uPA$^{0/0}$) to yield SR-uPA$^{+/0}$ and SR-uPA$^{0/0}$ littermate controls. We used aortas of four 20-week-old mice (both SR-uPA$^{+/0}$ and SR-uPA$^{0/0}$) to further develop protein extraction techniques; the remaining experimental mice (n=93, plus 18 bone marrow donors) are described in detail below. We used only female experimental mice because the accelerated atherosclerosis and plaque-rupture phenotypes that we investigated here were described in female mice.[27, 29] These phenotypes have never been investigated in males. All mice were housed in a specific-pathogen-free facility, and genotyped by PCR for the SR-uPA allele.[27]

To generate a first set of samples for proteomic analyses, 5-week-old SR-uPA$^{+/0}$ (n=12) and SR-uPA$^{0/0}$ (n=13) littermates were fed a diet containing 21% fat and 0.15% cholesterol by weight (TD88137; Harlan-Teklad). One SR-uPA$^{+/0}$ mouse died before its planned harvest. After 15 weeks on diet, proximal thoracic aortas (described in more detail below) were harvested and were either frozen immediately (6 SR-uPA$^{+/0}$ and 6 SR-uPA$^{0/0}$) or were explanted and cultured to generate conditioned medium (5 SR-uPA$^{+/0}$ and 7 SR-uPA$^{0/0}$). Two of the SR-uPA$^{0/0}$ samples were later excluded for technical reasons (evidence of

significant blood contamination in 1 sample and low peptide counts in a second sample), leaving 5 conditioned medium samples per group.

A separate cohort of SR-uPA$^{0/0}$ mice (n=68) was maintained on a normal laboratory diet until 35 weeks of age, then lethally irradiated with 10.5 Gy (Cesium-137 gamma-ray source) and transplanted by tail vein injection of approximately 1.2×10^7 bone marrow cells from 12–19-week-old donors. Forty-five mice received bone marrow transplants (BMT) from SR-uPA$^{+/0}$ donors (n=10 donors) and 23 mice received BMT from SR-uPA$^{0/0}$ donors (n=8 donors). BMT recipients received neomycin-containing water (2 mg/mL) for 1 week before and 2 weeks after BMT and were maintained on a normal laboratory diet post BMT. Mice were enrolled as BMT recipients only if they appeared in excellent health. After enrollment, mice were not randomized between the 2 BMT donor genotypes because of their genetic homogeneity and their uniformly healthy appearance at the time of BMT. Allocation concealment was also not performed because the experimenter was aware of which bone marrow genotype the next enrollees were going to receive. However, this awareness came only at a late stage: as BMT recipients aged toward 35 weeks, their treatment allocation was determined by availability of donor mice of each BM genotype and whether enrollment in one or the other group had been completed. In addition, the genetic homogeneity of the BMT recipients, their uniformly healthy condition, and the severe phenotype resulting from BMT with the experimental (SR-uPA$^{+/0}$) vs. control (SR-uPA$^{0/0}$) bone marrow make it highly unlikely that lack of allocation concealment would alter the results. After BMT, mice were monitored for signs of distress such as inactivity and failure to groom. Twelve SR-uPA$^{+/0}$ BMT recipients and 2 SR-uPA$^{0/0}$ BMT recipients died or were euthanized (due to deteriorating health) before their planned harvests (8 weeks post BMT). Aortas were harvested from 33 SR-uPA$^{+/0}$ BMT recipients and 21 SR-uPA$^{0/0}$ BMT recipients.

The individual responsible for enrolling mice, performing BMT, harvesting aortas, and collecting conditioned medium was not blinded to bone marrow donor genotype. Lack of blinding was due to practical considerations (to avoid mixing up experimental and control mice) and to our assessment based on previous studies that the severe phenotype engendered by transplantation of SR-uPA$^{+/0}$ bone marrow was unlikely to be altered by minor variations in handling of the mice and their tissues. We did not perform formal sample size and power calculations before commencing the study. Instead, the number of mice enrolled was selected prospectively based on a goal of achieving n=6 in all experimental groups. Selection of n=6 was based on our extensive experience with tissue proteomics, as well as our expectation that pooled samples would be needed in order to generate a sufficient amount of protein for PROTOMAP. The number of human plaques selected for protein extraction and analysis was also set prospectively at 6. In both cases, members of the team with experience in proteomic analyses suggested that use of 6 independent biological replicates would be adequate to detect biologically important differences in the vascular proteome. Mice were housed in a specific-pathogen-free facility in cages with absorbent bedding (Natural Absorbent 1/4” Bed-o’Cobs; Andersons Lab Bedding). All animal protocols and procedures were approved by the University of Washington Office of Animal Welfare.

Studies on human carotid plaques.

Patients scheduled for carotid endarterectomy at the University of Washington Medical Center, Harborview Medical Center, or the VA Puget Sound Health Care System provided informed consent for their tissues to be studied and for de-identified clinical information to be abstracted from their medical records. Inclusion criteria for the study were: preoperative for carotid endarterectomy, medically stable, age 50–80, English-speaking, willing to participate in study, and able to give informed consent before the day of surgery. Potential subjects at the VA Puget Sound Health Care System were excluded if they were already enrolled in a different (imaging-based) study to which their surgically removed carotid plaques were already committed. There were no other specific exclusion criteria. All protocols involving human subjects were approved by the Human Subjects Division of the University of Washington and the Institutional Review Board of the VA Puget Sound Health Care System.

Processing of mouse aortic tissue and generation of aorta-conditioned medium.

At the time of harvest (15 weeks after initiating the high-fat diet, for mice not receiving BMT; 8 weeks after BMT for the BMT recipients) mice were anesthetized with ketamine (140 mg/kg) and xylazine (40 mg/kg), saline perfused, and exsanguinated via cardiac puncture. For mice not receiving BMT, the proximal thoracic aorta was removed from the point at which it exits the heart to a point halfway between the left subclavian artery and the diaphragm. For BMT recipients, the same aortic segment was removed, with the innominate artery attached. Aortic segments destined for protein extraction were trimmed free of periadventitial fat in situ, excised, then snap frozen in liquid nitrogen, and stored at –80 °C. To obtain aortic segments for explant culture, mice were anesthetized and perfused in the same manner. Aortas were trimmed in situ, excised (from aortic root to midway between the left subclavian artery and the diaphragm, without attached innominate), washed 3 times at 37 °C in 2 mL of M199 (Gibco 11043–023; 20 minutes per wash), then placed in wells of a 96-well plate in 110 μL of M199 medium at 37 °C. After 20 hours, the conditioned medium was collected and stored at –80 °C.

Human plaque harvest and processing.

A total of 22 carotid plaques were removed in the operating room as part of a clinically indicated procedure. Freshly removed plaques were placed in a tube containing ice-cold PBS with 25 mM EDTA, 1x HALT protease-inhibitor cocktail (Pierce Biotechnology, #87786) and 1x HALT phosphatase-inhibitor cocktail (Pierce Biotechnology, #78420) and transported to the laboratory. As part of the surgical procedure, some plaques were divided with a single axial incision that opened up the vessel lumen. Other plaques arrived intact and were divided axially via a single incision extending through the common carotid segment then through the internal carotid artery segment. The specimens were then rinsed 5 times with 50 mL ice-cold PBS, placed in the inverted lid of a tissue culture dish with the axial incision facing upwards, and covered with ice-cold PBS with protease and phosphatase inhibitors/EDTA.

Using forceps for traction, we then exposed the lumen of the carotid plaque and examined the lumen surface for presence of an ulcerated lesion with thrombus/hemorrhage (a

"ruptured" plaque). Such lesions were typically located at the bifurcation, opposite the external carotid artery take-off. Plaques without gross evidence of rupture were not studied further. The area with the ulcerated lesion, including the full thickness of the plaque specimen below it, was trimmed with a scalpel to remove tissue adjacent to the ulcerated lesion. These "ruptured" plaque specimens were typically rectangular solids, with sides of ~0.5–1.0 cm and a thickness of ~1 mm. If the ulcerated area was large, we divided it into 2 pieces, to provide a backup sample in case we encountered technical difficulties extracting and analyzing the first sample. A scalpel was then used to cut one thin, full-thickness slice from both the caudal and cranial ends of each sample. These slices of ruptured plaque tissue were placed in 10% formalin for 48 hours, then stored in 70% ethanol for later histological analysis. The remainder of the ruptured plaque specimens was snap-frozen in liquid nitrogen and stored at –80 °C for later protein extraction. To select "stable" plaque tissue, we then examined the lumen of the remaining plaque tissue to locate areas that did not have surface ulceration, thrombosis, or hemorrhage and could be easily dissected free. These areas were typically at or near the caudal end of the specimen, and often included tissue from the common carotid artery. Segments of this plaque area ("stable" plaque tissue) —approximately equal in surface area to the ruptured specimen, but thinner (<1 mm)—were dissected free. If possible, more than 1 stable segment was dissected free per sample. A scalpel was used to cut thin slices from the caudal and cranial ends of these stable plaque specimens and the slices were placed in 10% formalin for 48 hours, then transferred to 70% ethanol. The remainder of the stable plaque specimens were snap-frozen in liquid nitrogen and stored at –80 °C for later protein extraction.

We initially collected 16 carotid plaques. One plaque was delivered as a fragment and was excluded from further study. On gross examination, 8 plaques did not show any evidence of luminal thrombosis, 1 plaque had equivocal evidence of luminal thrombosis and 1 plaque had only a small area of luminal thrombosis; all were excluded. Extracts of the remaining 6 ruptured plaques (and of adjacent stable plaque tissue) were analyzed using shotgun proteomics. We planned to analyze these same extracts using PROTOMAP; however, the extracts were lost in a laboratory accident. Therefore, we collected an additional 6 carotid plaques. Extracts of this second set of 6 plaques—plus new extracts of back-up ruptured and stable segments of 1 plaque from the first set of 6 plaques—were processed for PROTOMAP analyses. Because of technical issues (e.g., disconnected tubing resulting in sample loss), only 5 of these 7 samples yielded PROTOMAP data. Extracts of the second set of 6 plaques were also analyzed with shotgun proteomics as a "validation cohort" for discoveries made with the first set of 6 plaques.

Protein extraction from tissues.

To develop a method that would enrich the extracts in ECM proteins, we tested 2 tissue extraction protocols. According to the first protocol (P1; similar to a published protocol),[32] frozen tissue was pulverized in liquid nitrogen and resuspended in 20 mM phosphate buffer pH 7.0 with 10 mM EDTA, 1x HALT protease-inhibitor cocktail, and 1x HALT phosphatase-inhibitor cocktail. The suspension was incubated at 37 °C for 10 minutes then centrifuged at 12,000 g for 15 minutes at 4 °C. The supernatant (Fraction 1; termed P1F1) was stored at –80 °C. The pellet was resuspended in 4M Guanidine HCl in 50 mM acetate

buffer (pH 5.8), incubated overnight on a rotator at 4 °C, then spun at 16,000 g for 15 minutes at 4 °C. The supernatant (Fraction 2; termed P1F2) was dialyzed against distilled water at 4 °C overnight and either stored at –80 °C (for shotgun proteomics) or lyophilized (for PROTOMAP).

According to the second protocol (P2), frozen tissue was pulverized in liquid nitrogen and resuspended in ice-cold 50 mM Tris 10 mM EDTA (pH 8.0) with 1X HALT protease-inhibitor cocktail and 1X HALT phosphatase-inhibitor cocktail. The suspension was homogenized through sonication on ice: 3 cycles of 10 sec on/10 sec off, 5 min on ice, then another 3 cycles of sonication (10 sec on/10 sec off), using a sonic dismembrator (Fisher Scientific, #FB120) at an amplitude setting of 40%. The suspension was then centrifuged at 100,000 g for 45 minutes at 4 °C. The supernatant (Fraction 1, termed P2F1) was stored at –80 °C. The pellet was resuspended in ice-cold 50 mM Tris 10 mM EDTA (pH 8.0) and sonication was performed followed by centrifugation, as for Fraction 1. The resulting supernatant (Fraction 2, termed P2F2) was stored at –80 °C.

Because pilot experiments testing the protocols described above showed that the P1F2 fraction contained the largest number of ECM proteins (see Results)), we used the P1 protocol to extract protein from experimental mouse aortas and from human carotid plaques, and performed all proteomics analyses on Fraction 2. For mice that did not receive BMT, individual aortas (n=12) were extracted and extracts analyzed individually. For mice that received BMT, individual aortas (n=54) were pooled into groups of 3 and extracted (33 aortas from SR-uPA$^{+/0}$ recipients were pooled to generate 11 samples; 21 aortas from SR-uPA$^{0/0}$ recipients were pooled to generate 7 samples). We pooled samples in order to have sufficient protein for both shotgun proteomics and PROTOMAP analyses. For both SR-uPA$^{+/0}$ and SR-uPA$^{0/0}$ BMT recipients, the 6 pooled samples with the highest amounts of protein were used for proteomics analyses; other samples were not analyzed.

Sample processing and shotgun proteomics analysis.

The concentration of protein in aortic and carotid extracts was measured with the Bradford assay. For trypsin digestion, an aliquot of protein extract corresponding to 10 μg of protein was diluted first to 50 μL with 100 mM ammonium bicarbonate and subsequently with 1% RapiGest (Waters 186001861) in 100 mM ammonium bicarbonate to 100 μL (final concentration 0.5% RapiGest). Samples were then denatured and reduced with 5 mM DTT by heating at 65 °C for 1 h, and alkylated with 15 mM iodoacetamide (30 min at room temperature in the dark). Excess iodoacetamide was quenched with additional 5 mM DTT and the sample was digested with trypsin (Promega, V5111) at 1:20 w/w ratio overnight at 37 °C with mixing. After digestion, RapiGest was hydrolyzed by addition of 1% trifluoroacetic acid and the pellet was separated by centrifugation at 14,000 g for 10 min. The samples were desalted by solid phase extraction using Oasis HLB 96-well μElution Plate, dried down and stored at –80 °C until LC-MS analysis. Before analysis, samples were reconstituted with 0.1% formic acid (FA) in 5% acetonitrile to a concentration of 0.2 μg/μL.

The digested peptides (0.3 μg for lysates) were injected on a trap column (in-house packed 40 × 0.1 mm, 5 μm XBridge BEH C18, Waters), desalted for 5 min at a flow of 4 μL/min and separated on a pulled tip analytical column (in-house packed 280 × 0.075 mm, XBridge

BEH C18, 3.5 μm, Waters) heated to 50 °C with a 3-segment linear gradient of acetonitrile, 0.1% FA (B) in water, 0.1% FA (A) as follows: 0–5 min 1–10% B, 5–155 min 10–25% B, 155–185 min 25–35% B, followed by column wash at 80% B and reequilibration at a flow rate 0.4 μL/min (Waters NanoACQUITY UPLC). Tandem MS/MS spectra were acquired on Orbitrap XL (Thermo Scientific) operated in data-dependent mode on charge states 2–4 with 8 MSMS scans with dynamic exclusion for 30 s, CID fragmentation (NCE 35%) and MSMS acquisition in the linear ion trap. MS spectra were acquired at resolution 60,000 in the Orbitrap, and MSMS spectra (precursor selection window 2.0 Da) were acquired in the linear ion trap. Peptides and proteins were identified using the Comet search engine,[33] with PeptideProphet and ProteinProphet validation[34, 35] (search criteria included 20 ppm tolerance window for precursors and nominal resolution for products, Cys alkylation and Met oxidation as fixed and variable modifications, respectively). Except for analyses performed during method development, we applied stringent protein identification criteria: protein identifications were considered valid only if at least 3 unique peptide-spectrum matches (PSM) were detected in at least 4 samples in an analyzed group of experimental or control samples. Proteins that failed this test were not included in later analyses. Even after applying this test, some of the identified proteins were not detected in all of the samples. For samples in which a protein was not detected, we used 0 for the number of PSM for that protein.

Relative quantification of proteins was accomplished using spectral counting and the PepC statistical approach (PepC version 1.0.).[36] We used PepC, a statistical procedure developed for proteomic data analysis and validated in multiple studies[36–39] as a method for identifying proteins that are differentially abundant between groups of tissue extracts or between groups of tissue culture medium. PepC combines dual statistical tests, t-test and G-test, with random permutation testing to allow computation of false discovery rates (FDR). Before applying the PepC algorithm, the measured PSMs for each protein were normalized to the total PSMs across all proteins in that sample. Individuals responsible for performing the proteomics experiments and for the initial analyses of proteomics data were blinded both to mouse genotype and to whether individual plaque extracts were from ruptured or stable areas.

Sample processing and analysis by PROTOMAP approach.

100 μg of each protein sample were separated via a 10% SDS-PAGE gel for 850 volt hours. The gel was washed in water and manually excised into 0.5 cm bands. Bands which corresponded to the migration of molecular-weight markers were noted and this information was used to estimate the molecular weights of proteins migrating in each band. Bands were subjected to in-gel trypsin digestion as previously described.[30] Briefly, bands were washed in 100 mM ammonium bicarbonate and proteins were reduced in 10 mM tris(2-carboxyethyl) phosphine (TCEP) at 37 °C for 0.5 hr and then alkylated with 55 mM iodoacetamide in the dark for 0.5 hr. The bands were then dehydrated by washing in 1:1 acetonitrile:100 mM ammonium bicarbonate. Gel bands were then dried and resuspended in 40 μL of trypsin at 10 ng/μL. Upon re-swelling of the gel bands, 25 mM ammonium bicarbonate was added to a final volume of 200 μL and the gel bands were placed at 37°C overnight. Supernatants containing peptides were removed, and the gel bands were further extracted with 5% formic acid and acetonitrile. The pooled supernatants were dried and

stored at –80 °C until analysis. Prior to analysis, samples were resuspended in 10 μL buffer A (95% H_2O, 5% acetonitrile, 0.1% formic acid) and autosampler loaded onto a 100 μm (inner diameter) fused silica capillary column with a 5 μm tip containing 10 cm of C18 resin (Aqua 5 μm, Phenomenex).

LC-MS/MS analysis was performed on an LTQ ion trap mass spectrometer (ThermoFisher) coupled to an Agilent 1100 series HPLC. Peptides were eluted from the column using a 2-hour gradient of 5–100% Buffer B (Buffer B: 20% H_2O, 80% acetonitrile, 0.1% formic acid). The flow rate through the column was 0.25 μL/min and the spray voltage was 2.5 kV. The LTQ was operated in data-dependent scanning mode, with one full MS scan (400–1,800 m/z) followed by an MS^2 scan of the most abundant ion, followed by an MS^2 scan of the 2^{nd} most abundant ion, sequentially through the 7^{th} most abundant ion, with dynamic exclusion enabled (20 s duration). A subset of the human plaque samples was analyzed on an LTQ-Velos Elite Orbitrap mass spectrometer (ThermoFisher) coupled to an Agilent 1200 series HPLC in similar fashion to the ones described above, but the full MS scan (120,000 resolution) was followed by twenty MS^2 scans of the top 20 most abundant ions with dynamic exclusion enabled (20 s duration).

PROTOMAP data collection and analysis.

The mass spectrometry proteomics data have been deposited to the ProteomeXchange Consortium via the PRIDE[40] partner repository with the dataset identifiers PXD020405 and PXD020406. Raw mass spectrometry data were converted to MS2 format using RawXtract (version 1.9.9.2).[41] Peptide spectral matching was accomplished with ProLuCID.[42] ProLuCID was configured to allow for differential oxidation of methionine (16 or 15.9949 amu for LTQ or Elite, respectively) and required cysteines to be carboxamidomethylated (+ 57, 57.0215 amu for LTQ or Elite, respectively). The data were searched using a human or mouse reverse-concatenated non-redundant (gene-centric) FASTA database that was assembled from the UniProt database (http://www.uniprot.org/) downloaded on 11/5/2012 or 11/9/2012, respectively. The resulting matched MS2 spectra were assembled into protein identifications and filtered using DTASelect (version 2.0.47) using default settings. The data were then processed using custom perl scripts as previously described.[30] For each resulting peptograph, spectral counts were averaged for each band and condition and displayed with error bars representing standard errors of the mean.

Individual proteins were identified by PROTOMAP if at least 20 total spectral counts were detected among all of the samples analyzed. To use the PROTOMAP M.W. COMPARE tool to identify proteins with a shift in average migration on SDS-PAGE between extracts of experimental and control samples, we used a spectral count minimum of 20 per protein and a minimum average migration shift of 3 bands between experimental and control samples. To use the PROTOSORT algorithm to identify proteins that display changes in abundance and/or migration, we used a fold-change of 3 between the experimental and control samples, a mimimum of 10 spectral counts for the fragment to be recognized, and a mimimum of 25 total spectral counts per protein.

Histology.

Slices of fixed human plaque tissue (2 slices from each of the ruptured and stable specimens) were processed into paraffin. From each tissue block, five 5-μm-thick sections were cut at eight 50-μm steps (5 sections, then 25 μm discarded tissue, then repeat × 7) covering a total of 400 μm. Hematoxylin and eosin and Masson's trichrome stains were performed on eight 50-μm step sections per tissue slice and were examined with the assistance of a vascular pathologist (R.F.N.). An observer blinded to specimen identity graded the slides for the presence or absence of intimal hemorrhage/thrombosis (i.e., extravascular red blood cells or fibrin clot, detected as a bright red intimal mass on trichrome-stained slides), cholesterol clefts, and calcification. Intimal hemorrhage/thrombosis was graded as definite (large amount of red blood cells/clot in intima), possible (small amount of free red blood cells in intima, either with minor cap disruption or no cap disruption; thought potentially due to processing artifact), or absent. Cholesterol clefts and calcification were graded as present or absent.

Immunohistochemistry.

Sections of both stable and ruptured human plaque segments described above were used for immunohistochemistry. All immunostaining was performed using a Leica BOND RX Automated IHC Research Stainer, with reagents from Leica Biosystems except as indicated. Initial studies were performed only with sections of stable plaques, with the goal of localizing LAMA5, HSPG2, and COL18A1 and confirming that these proteins are present in caps of advanced yet stable atherosclerotic lesions. For all slides, antigen retrieval was performed with proteinase K for 15 minutes at 37 °C. Primary antibodies and dilutions were: rabbit anti-mouse laminin α5 serum (clone 504; a gift from Dr. Lydia Sorokin, Munster University; 1:1000),[43] mouse monoclonal anti-mouse endostatin (a fragment of COL18A1; Santa Cruz Biotechnology sc-32720; 1:100), and rat monoclonal anti-HSPG2 (Abcam ab2501; 1:100). Negative control primary antibodies and dilutions were: rabbit IgG (R&D Systems AB-105-C; 1:1000), mouse IgG (Mouse Negative Control Clone MOPC-21; PA0996; 1.7 mg/L), and rat IgG2b K isotype Control (BD Biosciences 553986; 1:1000). Bound primary antibodies were detected with the anti-rabbit IgG Polymer Detection System, the anti-mouse IgG Polymer Detection System, and mouse-adsorbed unconjugated rabbit anti-rat IgG.

To test whether LAMA5 and HSPG2 were depleted in caps of ruptured human plaques, we performed additional immunohistochemical stains of sections of 3 ruptured human plaque segments and 1 stable human plaque segment, using antibodies validated by Rickelt and Hynes for use in immunohistochemistry.[44] Primary antibodies (mouse monoclonal anti LAMA5; AMAb91124; Atlas Antibodies and rabbit polyclonal anti HSPG2; Boster Biological Technology; PB9277) were applied at 1:250 and 1:750 dilutions, respectively. According to data provided by the manufacturers (available on product sheets), both of these antibodies detect the corresponding full-length proteins (400 kDa and 468 kDa, respectively). Negative-control primary antibodies are listed above. Primary antibodies were applied after antigen retrieval with the Leica HIER 2 reagent (EDTA; for LAMA5) or HIER 1 reagent (citrate; for HSPG2), with both solutions applied for 20 minutes at 100 °C. Bound LAMA5 antibody was detected with rabbit anti-mouse IgG, followed by incubation with

HRP-polymerized goat anti-rabbit IgG. Bound HSPG2 antibody was detected with HRP-polymerized goat anti-rabbit IgG. Peroxidase activity was detected with diaminobenzidine substrate and slides were counterstained with hematoxylin.

Immunoblotting.

We performed western blot analysis of tissue extracts from the same stable and ruptured human plaque segments (7 each) used for shotgun proteomics. For analysis of HSPG2 and LAMA5, 30 μg of the extracts were loaded onto 3–8% Tris acetate SDS-PAGE gels and transferred to nitrocellulose membranes. HSPG2 was visualized with 0.375 μg/mL of HSPG2 antibody (PB9277; Boster Biological Technology) in 5% milk/PBST overnight. LAMA5 was visualized with a 1:800 dilution of LAMA5 antibody (AMAb91124, Atlas Antibodies) in 5% milk/PBST overnight, after stripping the HSPG2 blot. For analysis of COL18A1 30 μg of the same tissue extracts were run on 4–12% Tris Glycine SDS-PAGE gel, transferred to a nitrocellulose membrane, and visualized with COLA18A1 antibody (ab207162 Abcam) diluted 1:1000 in 5% milk/PBST overnight. In all cases, bound antibody was detected with an appropriate secondary antibody coupled with HRP and SuperSignal™ West Femto Maximum Sensitivity Substrate (#34096, ThermoFisher Scientific).

Statistics.

We assessed the correlation of individual protein spectral counts among extracts of mouse aortas and extracts of human plaque segments by calculating pair-wise Spearman correlation coefficients. We applied correspondence analysis, a form of multidimensional scaling[45] as implemented in the TM4 software[46] (https://sourceforge.net/projects/mev-tm4/), to determine whether global variation in the ensemble of extracted proteins distinguished the 2 experimental groups of mouse aortas and the 2 experimental groups of human plaque segments. Multiple hypothesis testing was addressed using a permutation-based FDR analysis within the PepC algorithm and with an FDR threshold of <0.05 to determine significant differential abundance. PepC is sensitive to the distribution and dispersion of spectral counts. In the second shotgun proteomics study of human plaques, differences in abundance of 10 prospectively identified proteins were analyzed with the nonparametric Wilcoxon rank-sum test. To facilitate comparison of data sets, we also applied the Wilcoxon rank-sum test retrospectively to analyze differences in human and mouse ECM proteins that we had already identified as statistically significant using PepC, a method that controls for multiple hypothesis testing. Two-dimensional hierarchical clustering of differentially abundant proteins was performed and the primary branch point was used to segregate samples and proteins.[46]

For functional enrichment analyses, we used web-based programs (Webgestalt: http://www.webgestalt.org/ and Reactome: https://reactome.org/), along with proteins identified by PepC as differentially abundant. These programs use several databases: Gene Ontology (GO), Kyoto Encyclopedia of Genes and Genome (KEGG), Reactome, Disgenet, Mammalian Phenotype Ontology, Human Phenotype Ontology, and Online Mendelian Inheritance in Man (OMIM). Functional enrichment was determined using a hypergeometric test, and over-represented categories were identified after adjusting enrichment P-values for

multiple hypothesis testing using a strict FDR cutoff <0.01 (more-complete lists using FDR <0.05 are provided in the Online Tables).

By leveraging available gene-product interaction resources (https://analysis.ingenuity.com/pa/, https://string-db.org/), a protein interaction network[47, 48] was constructed based on differentially abundant proteins extracted from mouse aortas. To increase confidence in biological relevance, the connectivity among network members was limited to relationships based on experimentally verified direct interactions.

RESULTS

Development of a protocol to extract aortic extracellular matrix (ECM) proteins.

Because we hypothesized that plaque rupture is initiated by proteolysis of artery wall ECM, we developed a tissue-extraction protocol that maximizes extraction of arterial ECM proteins. We compared 2 protocols for their ability to extract ECM proteins, using rabbit aortas because they are larger than mouse aortas and therefore more suitable for protocol development. Both protocols (termed P1 and P2; see Methods) provide 2 protein fractions per sample (termed F1 and F2). Analysis of the 4 fractions (P1F1, P1F2, P2F1, and P2F2) using shotgun proteomics suggested that P1F2 was most enriched in ECM proteins (data not shown). To confirm this, we next compared P1 and P2 using thoracic aortas of *Apoe*$^{-/-}$ mice. We extracted 2 aortas with P1 and 2 aortas with P2, yielding 8 total samples (2 each of P1F1, P1F2, P2F1, and P2F2), and confirmed that the P1F2 fractions contained the largest number of unique proteins as well as the most unique proteins in the Gene Ontology (GO) category extracellular matrix (Online Data Set I). Of the 73 unique ECM proteins detected in any of the 4 fractions, 68 (93%) were present in P1F2 (Online Figure I). We therefore used the P1F2 fractions for all remaining mouse and human tissue analyses. Importantly, although the P1F2 fraction extracts were optimized for enrichment with ECM proteins, these fractions also contained many cell-associated proteins, as described below.

Proteomics of aortic extracts from SR-uPA$^{+/0}$ and SR-uPA$^{0/0}$ Apoe$^{-/-}$ mice.

To begin to discover how elevated protease expression alters the atherosclerotic plaque proteome, we extracted proteins from thoracic aortas of 20-week-old SR-uPA$^{+/0}$ and SR-uPA$^{0/0}$ mice (both *Apoe*$^{-/-}$; n=6 per group), and analyzed them by shotgun proteomics. This analysis identified 775 unique proteins (Online Data Set II). The relative abundance of individual proteins in the extracts was highly reproducible among the 12 samples with mean pairwise Spearman correlation coefficients of 0.86 (range 0.79–0.89) within each genotype and 0.78 (range 0.74–0.82) between the 2 genotypes.

Correspondence analysis based on variability in abundance across all 775 unique proteins clearly segregated SR-uPA$^{+/0}$ from SR-uPA$^{0/0}$ aortas, confirming global differences between the aortic proteomes of the two genotypes (Figure 1A). Using a previously validated statistical procedure (PepC),[36, 37] we detected significant differences in individual-protein abundance between the SR-uPA$^{+/0}$ and SR-uPA$^{0/0}$ aortas. One hundred proteins (13% of all identified proteins) were differentially abundant in SR-uPA$^{+/0}$ vs. SR-uPA$^{0/0}$ aortas at FDR<0.05 (Online Data Set II).[37] Proteins increased in SR-uPA$^{+/0}$ aortas included PLAU

as well as 2 other extracellular proteases that are involved in ECM remodeling (MMP2 and MMP3). Surprisingly, the remaining 58 more-abundant proteins included many intracellular proteins related to the cytoskeleton and cell adhesion (Table 1), suggesting that cytoskeletal structure and cell adhesion are altered in response to elevated vascular protease activity. Furthermore, elevated extracellular protease activity in SR-uPA$^{+/0}$ aortas[29] led to decreased abundance of numerous (25) aortic ECM proteins. Notably, 12 of the 25 (48%) were basement-membrane proteins (Table 1).

To obtain a more global view of the pathways that connect elevated vascular protease activity to plaque rupture, we performed unsupervised hierarchical cluster analysis on the 100 differentially abundant proteins (Figure 1B). We also interrogated multiple gene annotation, pathway, and mammalian disease databases, with a goal of applying functional enrichment analysis to the two distinct profiles that emerged from the cluster analysis. These analyses confirmed that the group of proteins significantly more abundant in SR-uPA$^{+/0}$ aortas was highly enriched in functional categories related to cell adhesion (e.g., adherens junction, focal adhesion, and cadherin binding; FDR<5×10^{-10} for all), cytoskeleton (e.g., actin cytoskeleton, cytoskeletal protein binding, cytoskeleton organization; FDR<2×10^{-4} for all) as well as immuno-inflammatory programs (e.g., signaling by interleukins, JAK-STAT signaling, and cytokine signaling; FDR<1.5×10^{-3} for all; Figure 1C and Online Data Set III, in which proteins in each over-represented category are listed). A review of functional categories over-represented among proteins that were less abundant in SR-uPA$^{+/0}$ aortas confirmed significant reductions in ECM and basement-membrane proteins (e.g., ECM organization, basement membrane, elastic fiber formation, basal lamina, and ECM proteoglycans; FDR<4×10^{-10} for all; Figure 1C and Online Data Set IV, in which proteins in each over-represented category are listed).

A protein-interaction network was built based on known direct interactions among the differentially abundant proteins (Figure 2 and Online Data Set V) and confirmed that the differentially abundant proteins that are associated with the extracellular space tended to have decreased abundance in SR-uPA$^{+/0}$ aortas; whereas, the differentially abundant proteins that are located in the cell membrane, cytoplasm, and nucleus tended to have increased abundance in SR-uPA$^{+/0}$ aortas. This observation was further corroborated by GO cellular component enrichment analysis (Online Data Sets III and IV). The protein-interaction network analysis also identified several densely connected hubs including FN1, MYH9, and ACTB that may represent drivers of the network's function.[49, 50] Although extracellular and structural proteins such as FN1, MYH9, and ACTB may not be thought of as likely network drivers, ample evidence from humans and mice suggests that alterations of extracellular and structural proteins can profoundly impact complex intracellular processes.[51–53] Collectively, these data indicate that PLAU overexpression in mouse atherosclerotic tissue—which can cause plaque rupture[29]—activates pro-inflammatory signals, depletes ECM components including basement-membrane proteins, and upregulates intracellular pathways related to cell-cell adhesion, cell-matrix adhesion, and the cytoskeleton.

Proteomics of medium conditioned by SR-uPA$^{+/0}$ and SR-uPA$^{0/0}$ aortas.

Several groups have investigated the pathogenesis of plaque rupture via proteomic analyses of the plaque "secretome" (i.e., proteins released in culture by explanted human plaques).[54–57] Therefore, as a complementary approach to our aortic tissue-extract analyses, we used the same shotgun proteomics methods to analyze the secretome of SR-uPA$^{+/0}$ and SR-uPA$^{0/0}$ aortas (n=5 per group). Proteomic analysis of aortic tissue culture medium (CM) detected 921 unique proteins (Online Data Set VI). This approach offered a distinct view of the aortic proteome, because nearly half of these proteins (431; 47%) were not identified in tissue extracts.

Statistical analysis with PepC revealed that 45 of the 921 proteins (4.9%) were differentially abundant (FDR<0.05) in CM of SR-uPA$^{+/0}$ vs. SR-uPA$^{0/0}$ explants. Functional enrichment analysis of the 45 differentially abundant CM proteins revealed—congruently with results obtained with aortic tissue extracts—that categories related to cell adhesion and cytoskeleton (e.g., focal adhesion, cell-substrate junction, adherens junction, and cytoskeleton) were significantly over-represented among proteins that were increased in SR-uPA$^{+/0}$ CM (FDR≤3×10^{-6} for all; Online Data Set VII, in which proteins in each over-represented category are listed). Functional categories related to apoptosis (e.g., apoptotic execution phase, apoptotic cleavage of cellular proteins, and apoptosis) were also significantly over-represented among proteins that were increased in SR-uPA$^{+/0}$ CM (FDR≤5×10^{-3} for all; Online Data Set VII). Also congruent with the aortic tissue extract data, ECM-related categories as well as other categories related to the extracellular space (e.g., extracellular space, ECM organization, blood coagulation, fibrinolysis, complement and coagulation cascades) were significantly over-represented among proteins that were less abundant in SR-uPA$^{+/0}$ CM (FDR≤10^{-5} for all; Online Data Set VIII, in which proteins in each over-represented category are listed).

Proteomics of aortic extracts from SR-uPA$^{+/0}$ and SR-uPA$^{0/0}$ bone marrow transplant (BMT) recipients.

Older SR-uPA$^{+/0}$ mice cannot be used to discover the impact of increased vascular protease activity on the proteome of more-advanced atherosclerotic lesions because SR-uPA$^{+/0}$ mice die suddenly between 10 and 30 weeks of age.[27] We therefore used a BMT approach and 35-week-old *Apoe*$^{-/-}$ recipients to determine how increased protease activity alters the proteome of advanced atherosclerotic lesions (which are present in innominate arteries of older *Apoe*$^{-/-}$ mice).[28, 58] Eight weeks after BMT from either SR-uPA$^{+/0}$ or SR-uPA$^{0/0}$ donors, we removed recipient innominate arteries (with proximal aortas attached), extracted proteins, and analyzed the extracts with shotgun proteomics. We included the proximal aorta because we were unable to extract sufficient protein from innominate arteries alone. Importantly, although lesions in these 43-week-old mice are more advanced than lesions in the 20-week-old SR-uPA$^{+/0}$ mice described above, the SR-uPA$^{+/0}$ BMT recipients are exposed to elevated levels of PLAU for a substantially shorter period of time (8 versus 20 postnatal weeks).

Analysis of aortic extracts of BMT recipients (n=6 samples per group, each pooled from 3 mice) revealed 1,465 unique proteins. PepC analysis identified 56 proteins that were

differentially abundant between SR-uPA$^{+/0}$ vs. SR-uPA$^{0/0}$ BMT recipients (3.8% of the total proteins identified; FDR<0.05; Online Data Set IX). Pathway analyses revealed that extracellular space was the only functional category that was over-represented among the 32 more-abundant proteins (FDR=8.5 × 10^{-5}; Online Data Set X, in which proteins in each over-represented category are listed). Functional categories significantly over-represented among the 24 less-abundant proteins also included extracellular space (FDR=4 × 10^{-8}; Online Data Set XI, in which proteins in each over-represented category are listed). Other categories over-represented among less-abundant proteins again included ECM as well as glycosaminoglycan binding, proteinaceous ECM, focal adhesion, and complement and coagulation cascades (FDR≤1 × 10^{-3} for all; Online Data Set XI).

Proteomics of ruptured and stable areas of human carotid artery plaques.

To determine whether the changes in protein abundance that we detected in the mouse models are also present in ruptured human plaques, we applied shotgun proteomics to extracts of ruptured and stable areas of carotid artery plaques removed from 6 individuals (12 total samples; all plaques were removed for clinical indications). Demographic and clinical characteristics of the 6 patients from whom these plaques were removed are in Online Table I (cohort 1). Histologic sections of ruptured and stable areas were examined for evidence of advanced atherosclerosis, including intimal hemorrhage/thrombosis, cholesterol clefts, and calcification (Figure 3). As expected, intimal hemorrhage/thrombosis was far more common in ruptured areas: sections from all 6 ruptured areas had either definite (5) or possible (1) intimal hemorrhage/thrombosis whereas none of the sections from stable areas showed definite intimal hemorrhage/thrombosis and only 1 showed possible intimal hemorrhage. Cholesterol clefts and calcification were equally common in sections from both ruptured and stable areas (~50% of sections in both groups showed cholesterol clefts, calcification, or both). Therefore, advanced atherosclerosis was present in all samples, but intimal hemorrhage/thrombosis was essentially confined to samples taken from areas judged by gross examination to be ruptured plaques.

Shotgun proteomics of the 12 plaque extracts identified 1,161 unique proteins (Online Data Set XII). Relative abundance of individual proteins in the extracts was highly reproducible among both the ruptured and stable samples, with mean pairwise Spearman correlation coefficients of 0.86 (range 0.79–0.90) among the stable samples and 0.80 (range 0.71–0.85) among the ruptured samples. In contrast, the relative protein abundance was much less correlated among the ruptured and stable samples: mean pairwise Spearman correlation coefficients of 0.60 (range 0.37–0.78). Correspondence analysis based on variability in abundance across all 1,161 proteins clearly segregated the ruptured and stable samples (Figure 4A). Differential protein abundance analysis using PepC found that 489 of the 1,161 proteins (42%) were differentially abundant between ruptured and stable areas. Among the 150 more-abundant proteins, only 1 (0.7%) was also more abundant in aortic extracts of 20-week SR-uPA$^{+/0}$ vs. SR-uPA$^{0/0}$ mice (HIST1H1B). Among the 339 less-abundant proteins, only 13 (4%) were also less abundant in aortic extracts of 20-week SR-uPA$^{+/0}$ vs. SR-uPA$^{0/0}$ mice. Strikingly, 7 of the 13 proteins that were significantly less abundant in both ruptured human plaques and SR-uPA$^{+/0}$ aortas were basement-membrane proteins (AGRN, HSPG2, LAMA5, LAMB2, LAMC1, NID1, and NID2), and another 4 of the 13

proteins were also ECM proteins (ELN, FBLN5, LTBP4, and MFAP4). The cell-surface laminin receptor (BCAM) was also less abundant in both SR-uPA$^{+/0}$ aortas and ruptured human plaques. Therefore, at the individual protein level, overlap between SR-uPA$^{+/0}$ aortas and ruptured human plaques is highly focused on a small number of basement-membrane and other ECM proteins.

Unsupervised hierarchical cluster analysis of the 489 differentially abundant proteins revealed distinct protein abundance patterns in ruptured vs. stable plaque areas (Figure 4B). Functional enrichment analysis further revealed that categories over-represented among proteins that were more abundant in ruptured areas (Figure 4C and Online Data Set XIV, in which proteins in each over-represented category are listed) included those related to inflammation (e.g., activation of immune response, acute inflammatory response, defense response, and complement activation; FDR<1×10^{-15} for all), atherosclerosis (e.g., arteriosclerosis and arterial occlusive disease; FDR<5×10^{-12} for both), blood coagulation (e.g., thrombosis, hemostasis, blood coagulation, and platelet degranulation; FDR<5×10^{-12} for all) and apoptotic cell clearance (FDR<6×10^{-3}). Similar to our results comparing aortas of SR-uPA$^{+/0}$ vs. SR-uPA$^{0/0}$ mice, categories over-represented among proteins that were less abundant in the ruptured areas included several ECM and basement-membrane protein-related categories (e.g., ECM, basement membrane, basal lamina, and laminin complex; FDR<8×10^{-5} for all; Figure 4C and Online Dat Set XIV, in which proteins in each over-represented category are listed). Other categories over-represented among less-abundant proteins included cell adhesion (adherens junction, focal adhesion, cell-substrate junction, cadherin binding, and integrin binding; FDR<2×10^{-8} for all), and cytoskeleton (cytoskeleton, actin cytoskeleton, regulation of cytoskeleton organization FDR<3×10^{-10} for all).

Despite little overlap at the individual protein level between the SR-uPA$^{+/0}$ model (i.e., 20-week-old transgenic mice) and ruptured human plaques, several of the functional categories that were over-represented among the differentially abundant proteins in ruptured human plaques overlap congruently with functional categories that were over-represented among the differentially abundant proteins in aortic extracts of SR-uPA$^{+/0}$ mice (Figure 1C and Figure 4C). This overlap between human and mouse results was particularly robust for functional categories related to the less-abundant proteins, including ECM and basement-membrant proteins (Table 2). Among proteins with increased abundance both in ruptured human plaques and in the SR-uPA$^{+/0}$ model, categories related to the immune response (e.g., interleukin-4 and −13 signaling) were highly over-represented. Among proteins with decreased abundance in both settings, categories related to the ECM and basement membrane were highly over-represented (e.g., ECM, proteinaceous ECM, ECM organization, ECM component, ECM proteoglycans, ECM binding, ECM structural constituent, basement membrane, basal lamina, laminin complex, elastic fiber formation, basal lamina, integrin binding, and cell adhesion-molecule binding; Figures 1C and 4C, Table 2, Online Data Sets III, IV, XIII, and XIV). However, enrichment patterns in some functional categories were discordant. For example, proteins in GO categories adherens junction, focal adhesion, and actin cytoskeleton were more abundant in SR-uPA$^{+/0}$ aortas but less abundant in ruptured human plaques (FDR<5×10^{-6} for all).

We also compared the human plaque proteomic data to results obtained with the mouse BMT model. Among the 150 more-abundant proteins in ruptured plaque segments, only 1 protein (0.7%) was also more abundant in aortic extracts of 20-week SR-uPA$^{+/0}$ vs. SR-uPA$^{0/0}$ BMT recipients (LTF). Among the 339 less-abundant proteins in ruptured plaque segments, only 6 (2%) were also less abundant in aortic extracts of 20-week SR-uPA$^{+/0}$ vs. SR-uPA$^{0/0}$ BMT recipients. Four of the 6 proteins are in the GO category ECM (ABI3BP, LTBP2, LTBP4, and MYL6), and 1 is an adhesion-plaque protein (ZYX); none were basement-membrane proteins. Compared to this small number of congruently abundant proteins, there was more substantial overlap in functional category over-representation between the human plaques and aortic extracts of the BMT recipients. The only category over-represented among more-abundant proteins in aortic extracts of SR-uPA$^{+/0}$ BMT recipients (extracellular space; FDR=8.5×10^{-5}) was also highly overrepresented among the more-abundant proteins in ruptured human plaques (FDR<1×10^{-15}). Ten of the 18 (56%) functional categories over-represented among less-abundant proteins in aortic extracts of SR-uPA$^{+/0}$ BMT recipients (Online Data Set XI; FDR<0.01 for all) were also over-represented among less-abundant proteins in ruptured human plaques (Online Data Set XIV; FDR<1×10^{-3} for all). These categories were again focused on ECM and included ECM, proteinaceous ECM, ECM organization, focal adhesion, collagen binding, glycosaminoglycan binding, and others.

PROTOMAP analysis of extracts of human carotid plaques and mouse aortas.

The reduced abundance of several structural ECM proteins—including basement-membrane proteins—in both SR-uPA$^{+/0}$ aortas and ruptured human plaques suggested that these proteins might be targets of proteolysis. We therefore analyzed the human plaque extracts with PROTOMAP, a proteomic analysis methodology that identifies proteolytic events and peptide fragments in complex protein mixtures.[30] For these analyses, we collected 6 additional carotid plaques (all removed for clinical indications; Online Table I, cohort 2) and extracted proteins from a ruptured area and a stable area of each plaque. We also extracted proteins from backup segments of one plaque from the first patient cohort (Online Table I, cohort 1). Technically satisfactory data were obtained for both ruptured and stable areas of 5 of the 7 plaques. Demographic and clinical characteristics of the 5 patients whose plaques yielded satisfactory PROTOMAP data are in Online Table I (cohort 3).

A total of 2,059 proteins were identified by PROTOMAP. Primary data are accessible at http://www.scripps.edu/cgi-bin/cravatt/pmap_project_page.pl?pname=Dichek (data set 161027 BvA). To detect evidence of increased proteolysis in ruptured vs. stable plaque segments—and to potentially identify proteolytic fragments that are markers of plaque rupture—we first used the PROTOMAP M.W. COMPARE tool to identify proteins with a shift in average migration on SDS-PAGE between extracts of ruptured and stable plaques. This tool identified 49 proteins with differential migration in ruptured vs. stable areas. However, only 5 of the 49 proteins had a higher average migration distance in the ruptured-plaque samples (i.e., a shift to lower molecular weight, suggestive of increased proteolysis). The remaining 44 proteins had a lower average migration distance (shift to higher molecular weight) in the ruptured-plaque samples.

We next used the PROTOSORT algorithm, which identifies proteins that display changes in abundance and/or migration. We hypothesized that increased proteolysis of structural ECM components (or other proteins) in ruptured plaques would yield more-abundant small peptides, with increased migration. We examined the peptographs (graphs of peptide abundance versus gel-slice number; a surrogate for molecular weight)[30] of the 593 candidate proteins identified by PROTOSORT. In most cases, the peptographs indicated that these proteins were identified by PROTOSORT based on differences in protein abundance. However, we also identified several proteins that appeared more fragmented in extracts of ruptured areas (e.g., CP, AGT, ITIH4, GPLD1, FA5, and SERPIND1) and a smaller number of proteins that appeared more fragmented in extracts of stable areas (e.g., LAMB2, SVIL; Online Table II and Figure 5A). Notably, although most of the proteins that appeared more fragmented in ruptured areas are in the GO category "extracellular space" and at least 2 are listed in GO categories related to ECM (cell-matrix adhesion and ECM organization for AGT; ECM for GPLD1), none of these proteins are structural ECM components.

To look more specifically for evidence of increased proteolysis of structural ECM proteins, we examined the peptographs of proteins extracted from the ruptured-plaque samples. We identified—among the 339 proteins found by shotgun proteomics to be significantly less abundant in ruptured areas of the first set of human plaque extracts (Online Data Set XII) —69 proteins that are in the GO category ECM (Online Table III). All 69 proteins were also identified by PROTOMAP analysis of the second set of plaque extracts. Concordant with data from the shotgun analyses, PROTOMAP tools found that 21 (30%) of these ECM proteins were significantly less abundant ($P<0.05$) in ruptured versus stable areas, and an additional 14 (20%) tended to be less abundant (i.e., $0.05\leq P\leq 0.2$) in ruptured areas (Online Table III). However, a review of all 69 peptographs (Figure 5B and data not shown) did not provide any additional evidence that these ECM components had undergone increased proteolysis in ruptured plaque tissue (i.e., we did not find increased abundance of low-molecular-weight peptides in ruptured plaque tissue).

We next repeated all of the PROTOMAP analyses described above on aortic extracts of SR-uPA$^{+/0}$ and SR-uPA$^{0/0}$ BMT recipients. As with the human plaque data, these analyses did not associate significant decreases in individual protein abundance (in aortas of SR-uPA$^{+/0}$ BMT recipients) with concomitant increases in small fragments of the decreased-abundance proteins. For example, of the 39 proteins found by shotgun proteomics to be significantly less abundant in SR-uPA$^{+/0}$ aortas (Online Data Set II), 36 were also identified by PROTOMAP in aortic extracts of SR-uPA$^{+/0}$ and SR-uPA$^{0/0}$ BMT recipients. Peptographs of these 36 proteins revealed only 1 protein (NID2) with a modest trend towards increased abundance of lower-molecular weight fragments in aortic extracts of SR-uPA$^{+/0}$ BMT recipients (Online Figure II).

Validation of decreased abundance of basement-membrane proteins in ruptured human plaques.

In parallel with the PROTOMAP analyses of human plaque extracts, we performed shotgun proteomics (Online Data Set XV) on extracts of the 6 new plaques initially collected for the PROTOMAP experiment; Online Table I, cohort 2). Because 7 basement-membrane

proteins were less abundant in both SR-uPA$^{+/0}$ aortas and in ruptured human plaques in the initial "discovery" cohort, we focused our analysis on these 7 proteins. We also focused on the 3 collagens that we had identified as less-abundant in ruptured vs. stable plaque segments of the discovery cohort (Online Data Set XII). Therefore, this second set of plaque extracts served as an independent "validation" cohort to test hypotheses generated from the first set of human plaque extracts. In agreement with the discovery cohort analysis, 5 of the 7 basement-membrane proteins were significantly less abundant in ruptured vs. stable segments (P<0.005 for LAMC1, LAMA5, LAMB2, and HSPG2; P<0.05 for NID1; Figure 6A) while the other 2 showed a strong trend towards decreased abundance (P<0.1 for AGRN and NID2). In contrast, of the 3 collagens, only COL18A1—which is a basement-membrane protein[59]—was also significantly less abundant in the validation cohort (P<0.005). Reanalysis of the mouse data using the Wilcoxon rank-sum test (Figure 6B) confirmed that all 7 of these basement-membrane proteins (and only COL18A1 of the 3 collagens) were significantly less abundant in SR-uPA$^{+/0}$ aortas (Figure 6B).

Immunoblotting of human plaque extracts.

We then used immunoblotting in an attempt to validate our mass-spectrometry-based detection of basement-membrane protein loss in ruptured human plaque segments. Loss of basement-membrane proteins was of particular interest because these proteins were decreased in both ruptured human plaques and in SR-uPA$^{+/0}$ aortas. Western blots of 7 paired protein extracts of stable and ruptured segments (1 from cohort 1; 6 from cohort 2) were probed to detect LAMA5 and HSPG2. Due to depletion of 1 sample, a separate blot of 6 paired extracts was probed to detect COL18A1 (Online Figure III). The LAMA5 antibody detected a band of ~400 kDa (consistent with intact LAMA5) in 6 of the 7 extracts of stable segments and in 0 of the 7 extracts of ruptured segments. Moreover, lower-molecular weight bands were more prominent in extracts of the ruptured-plaque segments. When the blot was probed with the HSPG2 antibody, higher-molecular-weight bands (~200–300 kDa) were again more prominent in the extracts of stable plaques, and lower-molecular-weight bands were more prominent in extracts of ruptured plaques. The immunoblot probed for COL18A1 revealed far more immunoreactive bands in extracts of ruptured versus stable plaques (consistent with increased proteolysis), although some of these fragments were of relatively high molecular weight. Bands corresponding to the molecular weight of the intact protein were not reliably detected on immunoblots for either HSPG2 or COL18A1.

Location of basement-membrane proteins in advanced human plaques.

To verify the presence and begin to determine the location of basement-membrane proteins that were revealed by mass spectrometry to be depleted in ruptured plaques (and were also depleted in SR-uPA$^{+/0}$ aortas), we performed immunohistochemistry on sections of stable segments of each of the 6 human plaques from cohort 1. We could not perform extensive or quantitative immunohistochemistry that compared stable and ruptured plaque tissue because nearly all of the ruptured plaque tissue was used for protein extraction, and only thin slices cut from the ends of the plaque segments were available for sectioning and staining. Moreover, most of the sections of ruptured plaques contained no plaque cap tissue. We stained the sections for LAMA5, HSPG2, and COL18A1 because these were the 3 most abundant basement-membrane proteins in the stable plaque segments, and all 3 were

significantly and substantially decreased in ruptured versus stable areas of both cohort 1 and cohort 2 (Figure 6A). All 3 proteins were abundant in the vascular media, but were also present in and around SMC-like cells in the plaque fibrous caps. LAMA5 and HSPG2 were also abundant in the endothelium/subendothelium; however, COL18A1 was detected in this location only rarely, and at apparently low levels (Online Figures IV and V).

Lastly, we attempted to confirm the loss of HSPG2 and LAMA5 from ruptured plaque tissue and localize loss of these basement-membrane proteins to the plaque fibrous caps. We focused on HSPG2 and LAMA5 because well-validated antibodies are available for detecting these proteins in tissue sections.[44] Importantly, both of these antibodies detect the corresponding full-length proteins on western blots (see Methods). Using sections stained with hematoxylin and eosin or Masson's trichrome, a vascular pathologist (R.F.N.) could locate small fragments of cap tissue in sections of only 3 of the ruptured plaques. Using adjacent slides, and a validated antibody to HSPG2,[44] we found only faint staining in the 3 ruptured-plaque cap fragments. In all 3 samples, the plaque cap fragments stained less intensely than adjacent vascular media (Online Figure VI; A–I). In contrast, sections from a stable plaque segment stained in parallel had strong staining for HSPG2 in the fibrous cap, with more faint staining in the vascular media (Online Figure VI; J–L). Parallel studies with a validated LAMA5 antibody[44] did not yield consistent results.

DISCUSSION

To identify the biological pathways through which increased vascular proteolysis leads to plaque rupture, to assess whether the SR-uPA$^{+/0}$ mouse model replicates biochemical features of human plaque rupture, and to gain new insights into the mechanisms of human plaque rupture, we performed proteomic analyses of atherosclerotic aortas of mice with macrophage-specific overexpression of PLAU (SR-uPA$^{+/0}$ mice) and of ruptured human carotid plaques. Our major findings are: (1) Germline overexpression of PLAU in atherosclerotic aortas of 20-week-old mice reproducibly alters the abundance of subsets of extractable aortic proteins and of proteins in the aortic secretome: ECM proteins are decreased; MMPs as well as proteins related to cell adhesion, cytoskeleton, inflammatory signaling, and apoptosis are increased. (2) Introduction of PLAU-overexpressing macrophages into advanced atherosclerotic mouse lesions (for 8 weeks) primarily alters extracellular proteins, including decreases in cell-adhesion and ECM proteins. (3) The proteome of a ruptured area of a human carotid plaque differs markedly from the proteome of adjacent stable plaque tissue: proteins related to inflammation, atherosclerosis, and blood coagulation are increased, whereas ECM, cell-adhesion, and cytoskeletal proteins are decreased. (4) Proteomes of atherosclerotic aortas of SR-uPA$^{+/0}$ mice and of ruptured human carotid plaques have limited overlap in the differential abundance of specific proteins, but show strikingly similar decreases in protein abundance within several ECM-associated functional categories and have congruent decreases in several individual basement-membrane proteins.

We initially generated SR-uPA$^{+/0}$ mice with a goal of developing a mouse model of protease-induced plaque rupture,[27] and later found that transplantation of SR-uPA$^{+/0}$ bone marrow into 35-week-old nontransgenic *Apoe*$^{-/-}$ recipients[28] reproduced critical histological

features of human plaque rupture.[29] We concluded that these histological findings—along with increased aortic PLAU and MMP activity in SR-uPA$^{+/0}$ BMT recipients—validated the SR-uPA$^{+/0}$ mouse as a model of protease-induced plaque rupture. However, this conclusion was based primarily on anatomic data. Other than documenting increased uPA and MMP activity in SR-uPA$^{+/0}$ aortas, we did not generate any biochemical data that might explain how increased proteolytic activity caused plaque rupture. We therefore conceived the present study to search for these biochemical data, and thereby identify molecular and cellular mechanisms underlying plaque rupture.

We designed the present study based on 3 assumptions: (1) that analyses of arterial tissue of 20-week-old SR-uPA$^{+/0}$ mice would reveal effects of increased protease activity on early mouse lesions; (2) that analyses of arterial tissue of SR-uPA$^{+/0}$ BMT recipients (8 weeks after BMT) would reveal effects of increased protease activity on more-advanced mouse lesions (including ruptured plaques); and (3) that analyses of ruptured human plaques would reveal the effects of increased protease activity on advanced human lesions. However, our results showed that alterations in the arterial proteome are far more extensive in aortas of 20-week-old SR-uPA$^{+/0}$ mice than in aorta/innominate arteries of the SR-uPA$^{+/0}$ BMT recipients. This observation, likely due to the longer duration of uPA overexpression in 20-week-old SR-uPA$^{+/0}$ mice, prompted us to analyze results from the 3 experiments according to the duration of exposure of plaque tissue to increased protease activity: SR-uPA$^{+/0}$ BMT recipients (8 weeks), SR-uPA$^{+/0}$ mice (20 weeks), then ruptured human plaques (>>20 weeks; Figure 7).

When analyzed in this manner, our proteomic data—from both SR-uPA$^{+/0}$ mice and ruptured human plaques—identify biochemical and cellular pathways that connect elevated vascular protease activity to plaque rupture. Aortas of mice exposed to elevated vascular protease activity for only 8 weeks (i.e., SR-uPA$^{+/0}$ BMT recipients) have relatively few differentially abundant proteins, predominantly located in the extracellular space. These aortas likely model the initiation of protease-mediated ECM degradation and cell-matrix detachment. In contrast, the aortas of mice exposed to elevated vascular protease activity for 20 weeks (i.e., SR-uPA$^{+/0}$ mice) have a far-larger number of differentially abundant proteins that include cell-associated as well as extracellular proteins. Our data suggest that this stage of plaque development likely models upregulation of cytoskeletal and cell-adhesion proteins in response to progressive ECM degradation. The hypothesis that upregulation of cytoskeletal and cell-adhesion proteins is a homeostatic cellular reaction to enhanced extracellular proteolysis is consistent with the observed global pattern of altered protein abundance in SR-uPA$^{+/0}$ aortas (Figure 2): proteins with decreased abundance are overwhelmingly extracellular, whereas proteins with increased abundance are overwhelmingly cell-associated. Moreover, this hypothesis is consistent with substantial in vitro data that connect extracellular proteolysis with alterations in cell-adhesion and cytoskeletal proteins.[60–64] The aortic proteome of 20-week-old SR-uPA$^{+/0}$ mice also shows elevated levels of apoptosis-related proteins, likely released from cells that are undergoing anoikis: programmed cell death that results from loss of cell-ECM contacts.[65]

The final biochemical steps associated with protease-mediated plaque rupture—that are not accessible in the germline transgenic SR-uPA$^{+/0}$ mice due to their premature deaths[27]

—are reflected in the proteome of ruptured human plaques (Figure 7). At this stage, matrix proteolysis has progressed and plaque cell death has occurred along with loss of endothelial barrier function and appearance of intraplaque hemorrhage and thrombosis. Accordingly, the human ruptured-plaque proteome is characterized by decreased levels of ECM proteins as well as cell-adhesion and cytoskeletal proteins, and increased levels of proteins associated with blood cells and clotting (e.g., hemoglobin, fibrinogen, and prothrombin). Taken together, our proteomic data map a temporal series of biochemical and cellular events in SR-uPA$^{+/0}$ aortas and human carotid plaques that lead from increased extracellular proteolysis to plaque rupture (Figure 7).

The present study was also designed to leverage proteomics to evaluate whether the SR-uPA$^{+/0}$ mouse model recapitulates key biochemical features of human plaque rupture. With few exceptions,[66, 67] mouse models of plaque rupture have been evaluated, promoted, and criticized based solely on their histologic—rather than their biochemical—resemblance to ruptured human plaques.[68–74] We are not aware of any mouse plaque-rupture studies in which biochemical data from the mouse model were compared directly with similar data generated from ruptured human plaques. Generation of data that enabled this comparison was challenging, because our SR-uPA$^{+/0}$ mouse proteomic data were largely from stable plaques (as any ruptured innominate artery plaques in tissue from SR-uPA$^{+/0}$ BMT recipients represent only a small fraction of the total extracted arterial tissue), whereas our human proteomic data were generated specifically from ruptured plaque tissue. Despite these limitations, our data strongly suggest that several key biochemical processes that are well described in unstable and ruptured human plaques—and are detected in our ruptured human plaques—are also present in atherosclerotic plaques of SR-uPA$^{+/0}$ mice. These processes include: elevated levels of MMPs and reduced levels of ECM proteins;[17, 18] activation of inflammatory pathways;[2, 13, 75, 76] and activation of apoptosis in association with ECM degradation.[77–79]

The overlap in biochemical processes between SR-uPA$^{+/0}$ aortas and ruptured human plaques is striking because—as mentioned above—comparison of differentially abundant proteins in 20-week-old SR-uPA$^{+/0}$ aortas with differentially abundant proteins in ruptured human plaques juxtaposes different disease stages and is therefore biased against finding common features. Indeed, there were few individual proteins that were commonly differentially abundant in both data sets: of the 100 differentially abundant proteins in the mouse data set and the 489 differentially abundant proteins in the human data set, only 27 proteins were differentially abundant in both. Nevertheless, these 27 proteins included several proteins in the GO category basement membrane that were significantly decreased in both data sets: AGRN, HSPG2, LAMA5, LAMB2, LAMC1, NID1, and NID2. These 7 basement-membrane proteins represent 18% of the 39 proteins that were significantly decreased in 20-week-old SR-uPA$^{+/0}$ mouse aortas, suggesting that basement-membrane loss is a biochemical feature of human plaque rupture that is particularly well modeled in SR-uPA$^{+/0}$ mouse aortas. We speculate that loss of basement-membrane proteins—most likely because of proteolysis—is an important and under-recognized contributor to plaque rupture.

We considered whether our results could shed light on whether human plaque rupture is driven by PLAU. If true, the SR-uPA$^{+/0}$ mouse—in which basement membrane protein loss and plaque rupture are definitely caused by elevated PLAU activity—would reproduce human disease even more closely. Others have hypothesized that human plaque PLAU activity precipitates rupture because PLAU is present in advanced human plaques, localizes at rupture-prone areas, and its abundance is correlated with plaque stability.[80–83] However, because measuring PLAU in human plaques was not an objective of this study, we did not optimize tissue processing protocols for detecting PLAU protein or activity. Accordingly, PLAU was not detected in human plaques by shotgun proteomics and was detected in only 1 sample by PROTOMAP analysis. It is, nevertheless, possible to use our results to propose a causal relationship between loss of specific basement-membrane proteins in ruptured human plaques and elevated plaque PLAU activity. Laminin, nidogen, HSPG2, and collagen XVIII are cleaved by plasmin, MMP9, or MMP12. These 3 proteases are elevated in ruptured human plaques and are activated either directly or indirectly by PLAU.[84, 85] Therefore our results are consistent with the hypothesis that elevated human plaque PLAU activity precipitates basement-membrane protein loss and plaque rupture, although our experimental methods cannot establish causality.

Basement-membrane protein loss due to pericellular matrix proteolysis could lead to plaque rupture via several mechanisms. The best-described mechanism involves SMC and EC apoptosis (anoikis) that is caused by loss of cell attachments to surrounding basement-membrane proteins.[7, 9, 77, 78, 86] Death of EC and SMC would weaken cap structure while also triggering a local inflammatory response that includes entry of protease-secreting inflammatory cells (e.g., macrophages,T-cells, and mast cells) to the artery wall.[7, 9] Proteolysis of sub-endothelial basement-membrane proteins such as laminins increases artery wall permeability, facilitating inflammatory cell entry,[87] and potentially increases lipoprotein entry as well. Migration and retention of inflammatory cells is further stimulated by basement-membrane proteolysis that releases chemotactic protein fragments and exposes adhesive protein domains (well decribed for laminins, agrin, other HSPGs, and nidogens).[88–90] Proteolysis of basement-membrane proteins can also shift SMC away from a contractile phenotype, weakening the fibrous cap.[91] A critical role for basement-membrane proteolysis that causes cap thinning and SMC death is supported by GWAS data that link coronary artery disease to a COL4A2 variant associated with lower COL4A1 and COL4A2 expression, increased SMC apoptosis, and fibrous cap thinning.[92] Other GWAS data associate SMC phenotypic modulation (a consequence of basement membrane proteolysis)[91] with unstable coronary artery disease.[93]

Loss of plaque fibrillar collagen—not of basement-membrane components—has long been considered a hallmark of human plaque rupture.[17, 18] Consistent with this, several functional categories related to collagen were over-represented among less-abundant proteins in both SR-uPA$^{+/0}$ aortas and ruptured human plaques, (e.g., collagen trimer in SR-uPA$^{+/0}$ aortas; FDR$<3 \times 10^{-3}$; and collagen binding in ruptured human plaques; FDR$<3 \times 10^{-4}$). However, at the individual protein level, no collagen molecule was decreased in both murine and human settings, and the number of less-abundant individual collagen molecules was small in both settings and non-overlapping: only COL14A1, COL18A1, and COL5A1 were lower in the discovery cohort of ruptured human plaques; only COL1A2, COL15A1, and

COL6A3 were lower in SR-uPA$^{+/0}$ aortas. Therefore, neither type I nor type III (i.e., fibrillar) collagen—thought to be the major vascular collagens providing tensile strength and resistance to plaque rupture[94–96]—were reduced in ruptured human plaques. Indeed, few collagen molecules were less abundant in ruptured versus stable plaque extracts: in the first set of human plaques, only 3 of 15 identified collagens were significantly reduced. In the second set, only 2 of 13 identified collagens were significantly reduced in ruptured plaques extracts, and 2 were significantly increased. In contrast to these modest changes in collagen abundance, several basement-membrane proteins were decreased in both settings (9 individual basement-membrane proteins in SR-uPA$^{+/0}$ aortas; 17 in the first set of ruptured human plaques; FDR$<2 \times 10^{-11}$ for basement membrane protein loss in both settings). Moreover, decreases in specific human basement-membrane proteins were highly reproducible in the second (independent) set of ruptured human plaques. Our unbiased proteomic data thus suggest that basement-membrane protein loss may be more critical than fibrillar collagen loss in promoting plaque rupture.

We also hypothesized that if ECM components were proteolyzed either in the SR-uPA$^{+/0}$ mouse or in ruptured human plaques, we would detect increased levels of proteolytic fragments in the corresponding tissue extracts. To address this question we used PROTOMAP, a technology designed to identify protease substrates and that relies, in part, on detection of elevated levels of substrate fragments.[30] Identification of these substrates might help both to identify the proteases that are responsible for plaque rupture and to identify peptide markers of plaque rupture.[24, 25] It is unclear why PROTOMAP did not identify ECM substrate fragments, especially because both SR-uPA$^{+/0}$ aortas and ruptured human plaques have significant increases in protease abundance and significant decreases of several ECM proteins. It is possible that protein fragments released during ECM proteolysis are: 1) rapidly cleared from the interstitial space; 2) unstable in arterial tissue in vivo; 3) inefficiently extracted from arterial tissue; or 4) lost during processing of the extracts. It is also possible that low size-resolution of the gel-LC (liquid chromatography) approach and inherent variability of in-gel digestion interferes with detection of proteolytic fragments. Additional work optimizing the extraction and identification of ECM peptide fragments is likely required before PROTOMAP can be used to identify the in vivo substrates of atherosclerotic plaque proteases.

We focused our study on identifying mechanisms of plaque rupture, because plaque rupture is the most common mechanism underlying coronary and carotid artery thrombosis.[4, 15] Plaque erosion can also precipitate coronary and carotid thrombosis, although it is a less common etiology of both.[4, 15] Because the design of our study precluded systematic histologic analysis of thrombosed human plaque tissue, we cannot exclude that some of our “ruptured” plaques may have been “eroded”. However, for two principal reasons, we believe it is unlikely that plaque erosion accounted for a majority of our thrombosed carotid plaques. First, in most clinical series examining thrombosed carotid plaques, plaque rupture is more common (60% in the largest study),[97] with plaque erosion estimated to be responsible for <25% of carotid plaque thrombosis.[4] Second, one of us (T.K.; unpublished data) recently completed a systematic histologic study of 111 carotid plaques collected at the same institutions as in the present study. Ruptured fibrous caps were present in 54% of the plaques, luminal surface disruption with mural thrombus was present in 36% of the

plaques, and some plaques had both features (as reported elsewhere).[15] Accordingly, it is highly unlikely that the thrombosed carotid segments studied herein were not predominantly ruptured plaques. Moreover, key biochemical features—including relatively low levels of ECM and SMC-specific proteins (e.g., ACTA2, MYH11, CNN1) along with high levels of proteins associated with atherogenic lipoproteins (APOB and APOE) were generally shared by all of the ruptured plaque segments. These biochemical features are more consistent with the substrate of plaque rupture versus plaque erosion.[76] These observations notwithstanding, a compelling argument has been made that basement-membrane proteolysis contributes importantly to plaque erosion as well as rupture.[9] According to this model, proteolysis of EC basement membrane would precipitate endothelial desquamation and plaque erosion, whereas proteolysis of the basement membrane surrounding SMC (especially fibrous-cap SMC) would trigger plaque rupture.[9, 98]

We were concerned whether the significant reductions in abundance of basement-membrane proteins in both the mouse and human studies were tightly linked to plaque-rupture processes (such as proteolysis) or whether they were driven primarily by other compositional differences between SR-uPA and nontransgenic mouse aortas and between ruptured and stable segments of human plaques. These other compositional differences could include increased macrophages and lipid in SR-uPA aortas[27] and increased plasma proteins in ruptured human plaque segments. Because these structural differences cannot be eliminated as experimental variables, this question may be impossible to answer. However, several observations argue that the lower abundance of basement-membrane proteins in ruptured human plaques is not driven by increased plasma protein abundance. First, as mentioned above, abundance of specific basement-membrane proteins is reproducibly lower in ruptured human plaques, but abundance of specific collagens is not. Second, if the decrease in basement-membrane proteins (as a percentage of total protein) in ruptured human plaque segments were due to accumulation of plasma proteins in ruptured plaque segments, immunoblots that detect basement-membrane proteins should show reproducible decreases in band intensities in extracts of ruptured versus stable plaque segments; yet they do not. Third, peptides derived from albumin (the most abundant plasma protein) are no more abundant in extracts of ruptured vs stable human plaque segments (mean 384 vs 337, P=0.54 in cohort 1; mean 806 vs 577, P=0.14 in cohort 2), discounting plasma protein abundance as a major uncontrolled variable.

Our study has several limitations. Unlike human plaques, mouse aortic plaques are too small to be specifically extracted, requiring that we extract proteins from larger segments of mouse aorta. These segments may contain areas without advanced atherosclerosis, diluting signals from the plaque-derived proteins. Similar considerations related to physical size prevented us from performing proteomic studies solely on innominate arteries of SR-uPA$^{+/0}$ BMT recipients, in which plaque rupture is common.[29] Interpretation of our human data must take into consideration that human plaques cannot be harvested immediately before they rupture, and that ruptured/thrombosed plaques removed in the operating room have already entered a healing phase, with corresponding changes in the plaque proteome. This limitation might be addressed in future studies in which proteomic analyses are performed on carotid plaques that are removed based on non-invasive assessment as high-risk, but have not yet ruptured.[99, 100] Our ability to use the proteomics data to identify novel pathways

and relationships is limited because our functional enrichment and network analyses are based on known biological processes and gene-product interactions. However, the primary aim of our analyses was to compartmentalize the complex molecular events occurring during plaque rupture within the context of well-defined canonical annotations and experimentally verified interactions. Another limitation is that our extraction protocol (developed with a focus on enrichment of ECM proteins) may not capture some important proteins and peptides. Absence of these proteins would limit comparison of our data with proteomic data generated by others, using different extraction methods.[25, 26] In addition, because the murine and human data exhibit only modest overlap in altered expression of individual proteins, our data suggest important differences between the biochemistry of SR-uPA$^{+/0}$ aortas and human carotid plaques. For example, the proteases that are more abundant in SR-uPA$^{+/0}$ aortas (MMP-2 and MMP-3) differ from the proteases that are more abundant in ruptured human plaques (MMP-9, MMP-12, MMP-19, neutrophil elastase, Cathepsins B, D, G, and Z, chymase, carboxypeptidase B2, carboxypeptidase N, and mast cell carboxypeptidase). Accordingly, development of pharmacologic strategies that target specific plaque proteases will need to rely on human rather than mouse data. Finally, proteolysis is the most likely cause of ECM loss from both SR-uPA$^{+/0}$ aortas and ruptured human plaques, and our immunoblots provide some support that ECM proteolysis is increased in ruptured plaque segments. However, a mass spectrometry-based assay (PROTOMAP) did not detect increased numbers of proteolytic fragments of the less-abundant ECM proteins. This could be a result of technical limitations of PROTOMAP methodology.

Unbiased discovery studies such as ours, which test numerous hypotheses simultaneously, risk generating falsely positive results, due only to chance. Concerns regarding false positivity are most definitively resolved when study predictions are borne out (e.g., through validation of our results by other groups using similar methodology or demonstration that interventions that alter basement-membrane proteolysis have predicted effects on plaque rupture). Nevertheless, we offer several reasons why our results are unlikely to be explained by chance: (i) we applied rigorous false-discovery rate threshholds to both the peptide-abundance data and the functional-enrichment data; (ii) in both murine and human studies, the statistical significance of over-representation of basement-membrane proteins among the decreased-abundance proteins was far below the FDR threshold ($P<2 \times 10^{-11}$ for both); (iii) 6 of the 7 basement-membrane proteins that were differentially abundant in both mouse samples and human cohort 1 were in the top 30% of differentially abundant proteins in cohort 1 (i.e., these were not “borderline” differences); (iv) the key findings on basement-membrane protein abundance in plaques from cohort 1 were reproduced independently in a second set of plaques (cohort 2). All 8 basement-membrane proteins (including COL18A1) were also decreased in this second set, with $P<0.005$ for 5 of the 8 proteins.

In summary, shotgun-proteomic studies performed with murine and human tissues identify biological pathways that link elevated vascular protease activity with plaque rupture and reveal that several biochemical features of human plaque rupture (e.g., inflammatory signaling, MMP abundance, decreased ECM proteins) are replicated in SR-uPA$^{+/0}$ mouse aortas. Our results also suggest that loss of basement-membrane proteins may play a central role in precipitating plaque rupture.

Supplementary Material

Refer to Web version on PubMed Central for supplementary material.

ACKNOWLEDGMENTS

We are grateful to Kristi Pimentel for help with human subject recruitment and to the University of Washington Histology and Imaging Core for assistance with histochemical staining. We thank Ilona Babenko for assistance with proteomics sample preparation and western blot analysis. This material is the result of work supported by resources from the VA Puget Sound Health Care System, Seattle, Washington.

SOURCES OF FUNDING

This work was supported by the National Heart Lung and Blood Institute grant (R21HL113405, to David A. Dichek), by the National Institute of Diabetes, Digestive, and Kidney Disease (P30DK017047, supporting the Quantitative and Functional Proteomics Core and the Cellular and Molecular Imaging Core of the University of Washington Diabetes Research Center), by the University of Washington Proteomics Resource (UWPR95794), and by the John L. Locke Jr. Charitable Trust. Sina Gharib was supported by the National Institute of Allergy and Infectious Disease (R01AI137111). Tomas Vaisar and Jay Heinecke were supported by P01HL092969 and P01HL128203. Jay Heinecke was supported by R01HL149685.

Nonstandard Abbreviations and Acronyms:

BMT	bone-marrow transplantation
CM	culture medium
ECM	extracellular matrix
FDR	false discovery rate
GO	gene ontology
MMP	matrix metalloproteinase
PROTOMAP	protein topography and migration analysis platform
PSM	peptide-spectrum match
SR-uPA	a transgene including the human scavenger receptor promoter and the mouse *Plau* gene

REFERENCES

1. Tabas I 2016 russell ross memorial lecture in vascular biology: Molecular-cellular mechanisms in the progression of atherosclerosis. Arterioscler. Thromb. Vasc. Biol 2017;37:183–189 [PubMed: 27979856]
2. Virmani R, Burke AP, Farb A, Kolodgie FD. Pathology of the unstable plaque. Prog. Cardiovasc. Dis 2002;44:349–356 [PubMed: 12024333]
3. Finn AV, Nakano M, Narula J, Kolodgie FD, Virmani R. Concept of vulnerable/unstable plaque. Arterioscler. Thromb. Vasc. Biol 2010;30:1282–1292 [PubMed: 20554950]
4. Kolodgie FD, Yahagi K, Mori H, Romero ME, Trout HHR, Finn AV, Virmani R. High-risk carotid plaque: Lessons learned from histopathology. Semin. Vasc. Surg 2017;30:31–43 [PubMed: 28818257]

5. Slager CJ, Wentzel JJ, Gijsen FJ, Thury A, van der Wal AC, Schaar JA, Serruys PW. The role of shear stress in the destabilization of vulnerable plaques and related therapeutic implications. Nat Clin Pract Cardiovasc Med 2005;2:456–464 [PubMed: 16265586]
6. Cheng C, Tempel D, van Haperen R, van der Baan A, Grosveld F, Daemen MJ, Krams R, de Crom R. Atherosclerotic lesion size and vulnerability are determined by patterns of fluid shear stress. Circulation 2006;113:2744–2753 [PubMed: 16754802]
7. Clarke MC, Figg N, Maguire JJ, Davenport AP, Goddard M, Littlewood TD, Bennett MR. Apoptosis of vascular smooth muscle cells induces features of plaque vulnerability in atherosclerosis. Nat. Med 2006;12:1075–1080 [PubMed: 16892061]
8. Wang J, Uryga AK, Reinhold J, Figg N, Baker L, Finigan A, Gray K, Kumar S, Clarke M, Bennett M. Vascular smooth muscle cell senescence promotes atherosclerosis and features of plaque vulnerability. Circulation 2015;132:1909–1919 [PubMed: 26416809]
9. Lindstedt KA, Leskinen MJ, Kovanen PT. Proteolysis of the pericellular matrix: A novel element determining cell survival and death in the pathogenesis of plaque erosion and rupture. Arterioscler. Thromb. Vasc. Biol 2004;24:1350–1358 [PubMed: 15191939]
10. Dunmore BJ, McCarthy MJ, Naylor AR, Brindle NP. Carotid plaque instability and ischemic symptoms are linked to immaturity of microvessels within plaques. J. Vasc. Surg 2007;45:155–159 [PubMed: 17210401]
11. Dickhout JG, Colgan SM, Lhotak S, Austin RC. Increased endoplasmic reticulum stress in atherosclerotic plaques associated with acute coronary syndrome: A balancing act between plaque stability and rupture. Circulation 2007;116:1214–1216 [PubMed: 17846339]
12. Maldonado N, Kelly-Arnold A, Vengrenyuk Y, Laudier D, Fallon JT, Virmani R, Cardoso L, Weinbaum S. A mechanistic analysis of the role of microcalcifications in atherosclerotic plaque stability: Potential implications for plaque rupture. Am J Physiol Heart Circ Physiol 2012;303:H619–628 [PubMed: 22777419]
13. Libby P The molecular mechanisms of the thrombotic complications of atherosclerosis. J. Intern. Med 2008;263:517–527 [PubMed: 18410595]
14. Shah PK. Molecular mechanisms of plaque instability. Curr. Opin. Lipidol 2007;18:492–499 [PubMed: 17885418]
15. Bentzon JF, Otsuka F, Virmani R, Falk E. Mechanisms of plaque formation and rupture. Circ. Res 2014;114:1852–1866 [PubMed: 24902970]
16. Newby AC. Proteinases and plaque rupture: Unblocking the road to translation. Curr. Opin. Lipidol 2014;25:358–366 [PubMed: 25089553]
17. Galis ZS, Sukhova GK, Lark MW, Libby P. Increased expression of matrix metalloproteinases and matrix degrading activity in vulnerable regions of human atherosclerotic plaques. J. Clin. Invest 1994;94:2493–2503 [PubMed: 7989608]
18. Sukhova GK, Schonbeck U, Rabkin E, Schoen FJ, Poole AR, Billinghurst RC, Libby P. Evidence for increased collagenolysis by interstitial collagenases-1 and −3 in vulnerable human atheromatous plaques. Circulation 1999;99:2503–2509 [PubMed: 10330380]
19. Deguchi JO, Aikawa E, Libby P, Vachon JR, Inada M, Krane SM, Whittaker P, Aikawa M. Matrix metalloproteinase-13/collagenase-3 deletion promotes collagen accumulation and organization in mouse atherosclerotic plaques. Circulation 2005;112:2708–2715 [PubMed: 16230484]
20. Schneider F, Sukhova GK, Aikawa M, Canner J, Gerdes N, Tang SM, Shi GP, Apte SS, Libby P. Matrix-metalloproteinase-14 deficiency in bone-marrow-derived cells promotes collagen accumulation in mouse atherosclerotic plaques. Circulation 2008;117:931–939 [PubMed: 18250269]
21. Quillard T, Tesmenitsky Y, Croce K, Travers R, Shvartz E, Koskinas KC, Sukhova GK, Aikawa E, Aikawa M, Libby P. Selective inhibition of matrix metalloproteinase-13 increases collagen content of established mouse atherosclerosis. Arterioscler. Thromb. Vasc. Biol 2011;31:2464–2472 [PubMed: 21903941]
22. Gough PJ, Gomez IG, Wille PT, Raines EW. Macrophage expression of active mmp-9 induces acute plaque disruption in apoe-deficient mice. J. Clin. Invest 2006;116:59–69 [PubMed: 16374516]

23. Chen YC, Huang AL, Kyaw TS, Bobik A, Peter K. Atherosclerotic plaque rupture: Identifying the straw that breaks the camel's back. Arterioscler. Thromb. Vasc. Biol 2016;36:e63–72 [PubMed: 27466619]
24. Stegemann C, Didangelos A, Barallobre-Barreiro J, Langley SR, Mandal K, Jahangiri M, Mayr M. Proteomic identification of matrix metalloproteinase substrates in the human vasculature. Circ Cardiovasc Genet 2013;6:106–117 [PubMed: 23255316]
25. Langley SR, Willeit K, Didangelos A, Matic LP, Skroblin P, Barallobre-Barreiro J, Lengquist M, Rungger G, Kapustin A, Kedenko L, Molenaar C, Lu R, Barwari T, Suna G, Yin X, Iglseder B, Paulweber B, Willeit P, Shalhoub J, Pasterkamp G, Davies AH, Monaco C, Hedin U, Shanahan CM, Willeit J, Kiechl S, Mayr M. Extracellular matrix proteomics identifies molecular signature of symptomatic carotid plaques. J. Clin. Invest 2017;127:1546–1560 [PubMed: 28319050]
26. Matic LP, Jesus Iglesias M, Vesterlund M, Lengquist M, Hong MG, Saieed S, Sanchez-Rivera L, Berg M, Razuvaev A, Kronqvist M, Lund K, Caidahl K, Gillgren P, Ponten F, Uhlen M, Schwenk JM, Hansson GK, Paulsson-Berne G, Fagman E, Roy J, Hultgren R, Bergstrom G, Lehtio J, Odeberg J, Hedin U. Novel multiomics profiling of human carotid atherosclerotic plaques and plasma reveals biliverdin reductase b as a marker of intraplaque hemorrhage. JACC Basic Transl Sci 2018;3:464–480 [PubMed: 30175270]
27. Cozen AE, Moriwaki H, Kremen M, DeYoung MB, Dichek HL, Slezicki KI, Young SG, Veniant M, Dichek DA. Macrophage-targeted overexpression of urokinase causes accelerated atherosclerosis, coronary artery occlusions, and premature death. Circulation 2004;109:2129–2135 [PubMed: 15096455]
28. Rosenfeld ME, Polinsky P, Virmani R, Kauser K, Rubanyi G, Schwartz SM. Advanced atherosclerotic lesions in the innominate artery of the apoe knockout mouse. Arterioscler. Thromb. Vasc. Biol 2000;20:2587–2592 [PubMed: 11116057]
29. Hu JH, Du L, Chu T, Otsuka G, Dronadula N, Jaffe M, Gill SE, Parks WC, Dichek DA. Overexpression of urokinase by plaque macrophages causes histologic features of plaque rupture and increases vascular mmp activity in aged apo e-null mice. Circulation 2010;121:1637–1644 [PubMed: 20351234]
30. Dix MM, Simon GM, Cravatt BF. Global mapping of the topography and magnitude of proteolytic events in apoptosis. Cell 2008;134:679–691 [PubMed: 18724940]
31. Dronadula N, Wacker BK, Van Der Kwast R, Zhang J, Dichek DA. Stable in vivo transgene expression in endothelial cells with helper-dependent adenovirus: Roles of promoter and interleukin-10. Hum. Gene Ther 2017;28:255–270 [PubMed: 27842439]
32. Didangelos A, Yin X, Mandal K, Baumert M, Jahangiri M, Mayr M. Proteomics characterization of extracellular space components in the human aorta. Mol Cell Proteomics 2010;9:2048–2062 [PubMed: 20551380]
33. Eng JK, Hoopmann MR, Jahan TA, Egertson JD, Noble WS, MacCoss MJ. A deeper look into comet--implementation and features. J. Am. Soc. Mass Spectrom 2015;26:1865–1874 [PubMed: 26115965]
34. Keller A, Nesvizhskii AI, Kolker E, Aebersold R. Empirical statistical model to estimate the accuracy of peptide identifications made by ms/ms and database search. Anal. Chem 2002;74:5383–5392 [PubMed: 12403597]
35. Nesvizhskii AI, Keller A, Kolker E, Aebersold R. A statistical model for identifying proteins by tandem mass spectrometry. Anal. Chem 2003;75:4646–4658 [PubMed: 14632076]
36. Heinecke NL, Pratt BS, Vaisar T, Becker L. Pepc: Proteomics software for identifying differentially expressed proteins based on spectral counting. Bioinformatics 2010;26:1574–1575 [PubMed: 20413636]
37. Becker L, Gharib SA, Irwin AD, Wijsman E, Vaisar T, Oram JF, Heinecke JW. A macrophage sterol-responsive network linked to atherogenesis. Cell Metab 2010;11:125–135 [PubMed: 20142100]
38. Reardon CA, Lingaraju A, Schoenfelt KQ, Zhou G, Cui C, Jacobs-El H, Babenko I, Hoofnagle A, Czyz D, Shuman H, Vaisar T, Becker L. Obesity and insulin resistance promote atherosclerosis through an ifngamma-regulated macrophage protein network. Cell Rep 2018;23:3021–3030 [PubMed: 29874587]

39. Kratz M, Coats BR, Hisert KB, Hagman D, Mutskov V, Peris E, Schoenfelt KQ, Kuzma JN, Larson I, Billing PS, Landerholm RW, Crouthamel M, Gozal D, Hwang S, Singh PK, Becker L. Metabolic dysfunction drives a mechanistically distinct proinflammatory phenotype in adipose tissue macrophages. Cell Metab 2014;20:614–625 [PubMed: 25242226]
40. Perez-Riverol Y, Csordas A, Bai J, Bernal-Llinares M, Hewapathirana S, Kundu DJ, Inuganti A, Griss J, Mayer G, Eisenacher M, Perez E, Uszkoreit J, Pfeuffer J, Sachsenberg T, Yilmaz S, Tiwary S, Cox J, Audain E, Walzer M, Jarnuczak AF, Ternent T, Brazma A, Vizcaino JA. The pride database and related tools and resources in 2019: Improving support for quantification data. Nucleic Acids Res 2019;47:D442–D450 [PubMed: 30395289]
41. McDonald WH, Tabb DL, Sadygov RG, MacCoss MJ, Venable J, Graumann J, Johnson JR, Cociorva D, Yates JR, 3rd. Ms1, ms2, and sqt-three unified, compact, and easily parsed file formats for the storage of shotgun proteomic spectra and identifications. Rapid Commun. Mass Spectrom 2004;18:2162–2168 [PubMed: 15317041]
42. Xu T, Park SK, Venable JD, Wohlschlegel JA, Diedrich JK, Cociorva D, Lu B, Liao L, Hewel J, Han X, Wong CCL, Fonslow B, Delahunty C, Gao Y, Shah H, Yates JR, 3rd. Prolucid: An improved sequest-like algorithm with enhanced sensitivity and specificity. J Proteomics 2015;129:16–24 [PubMed: 26171723]
43. Garbe JH, Gohring W, Mann K, Timpl R, Sasaki T. Complete sequence, recombinant analysis and binding to laminins and sulphated ligands of the n-terminal domains of laminin alpha3b and alpha5 chains. Biochem. J 2002;362:213–221 [PubMed: 11829758]
44. Rickelt S, Hynes RO. Antibodies and methods for immunohistochemistry of extracellular matrix proteins. Matrix Biol 2018;71–72:10–27
45. Fellenberg K, Hauser NC, Brors B, Neutzner A, Hoheisel JD, Vingron M. Correspondence analysis applied to microarray data. Proc. Natl. Acad. Sci. U. S. A 2001;98:10781–10786 [PubMed: 11535808]
46. Saeed AI, Sharov V, White J, Li J, Liang W, Bhagabati N, Braisted J, Klapa M, Currier T, Thiagarajan M, Sturn A, Snuffin M, Rezantsev A, Popov D, Ryltsov A, Kostukovich E, Borisovsky I, Liu Z, Vinsavich A, Trush V, Quackenbush J. Tm4: A free, open-source system for microarray data management and analysis. Biotechniques 2003;34:374–378 [PubMed: 12613259]
47. Calvano SE, Xiao W, Richards DR, Felciano RM, Baker HV, Cho RJ, Chen RO, Brownstein BH, Cobb JP, Tschoeke SK, Miller-Graziano C, Moldawer LL, Mindrinos MN, Davis RW, Tompkins RG, Lowry SF. A network-based analysis of systemic inflammation in humans. Nature 2005;437:1032–1037 [PubMed: 16136080]
48. Szklarczyk D, Morris JH, Cook H, Kuhn M, Wyder S, Simonovic M, Santos A, Doncheva NT, Roth A, Bork P, Jensen LJ, von Mering C. The string database in 2017: Quality-controlled protein-protein association networks, made broadly accessible. Nucleic Acids Res 2017;45:D362–D368 [PubMed: 27924014]
49. Barabasi AL, Gulbahce N, Loscalzo J. Network medicine: A network-based approach to human disease. Nat Rev Genet 2011;12:56–68 [PubMed: 21164525]
50. Schadt EE. Molecular networks as sensors and drivers of common human diseases. Nature 2009;461:218–223 [PubMed: 19741703]
51. Milewicz DM, Ostergaard JR, Ala-Kokko LM, Khan N, Grange DK, Mendoza-Londono R, Bradley TJ, Olney AH, Ades L, Maher JF, Guo D, Buja LM, Kim D, Hyland JC, Regalado ES. De novo acta2 mutation causes a novel syndrome of multisystemic smooth muscle dysfunction. Am J Med Genet A 2010;152A:2437–2443 [PubMed: 20734336]
52. Papke CL, Cao J, Kwartler CS, Villamizar C, Byanova KL, Lim SM, Sreenivasappa H, Fischer G, Pham J, Rees M, Wang M, Chaponnier C, Gabbiani G, Khakoo AY, Chandra J, Trache A, Zimmer W, Milewicz DM. Smooth muscle hyperplasia due to loss of smooth muscle alpha-actin is driven by activation of focal adhesion kinase, altered p53 localization and increased levels of platelet-derived growth factor receptor-beta. Hum. Mol. Genet 2013;22:3123–3137 [PubMed: 23591991]
53. Li DY, Brooke B, Davis EC, Mecham RP, Sorensen LK, Boak BB, Eichwald E, Keating MT. Elastin is an essential determinant of arterial morphogenesis. Nature 1998;393:276–280 [PubMed: 9607766]

54. Duran MC, Martin-Ventura JL, Mohammed S, Barderas MG, Blanco-Colio LM, Mas S, Moral V, Ortega L, Tunon J, Jensen ON, Vivanco F, Egido J. Atorvastatin modulates the profile of proteins released by human atherosclerotic plaques. Eur. J. Pharmacol 2007;562:119–129 [PubMed: 17336287]
55. de la Cuesta F, Barderas MG, Calvo E, Zubiri I, Maroto AS, Darde VM, Martin-Rojas T, Gil-Dones F, Posada-Ayala M, Tejerina T, Lopez JA, Vivanco F, Alvarez-Llamas G. Secretome analysis of atherosclerotic and non-atherosclerotic arteries reveals dynamic extracellular remodeling during pathogenesis. J Proteomics 2012;75:2960–2971 [PubMed: 22197968]
56. Rocchiccioli S, Pelosi G, Rosini S, Marconi M, Viglione F, Citti L, Ferrari M, Trivella MG, Cecchettini A. Secreted proteins from carotid endarterectomy: An untargeted approach to disclose molecular clues of plaque progression. J Transl Med 2013;11:260 [PubMed: 24131807]
57. Aragones G, Auguet T, Guiu-Jurado E, Berlanga A, Curriu M, Martinez S, Alibalic A, Aguilar C, Hernandez E, Camara ML, Canela N, Herrero P, Ruyra X, Martin-Paredero V, Richart C. Proteomic profile of unstable atheroma plaque: Increased neutrophil defensin 1, clusterin, and apolipoprotein e levels in carotid secretome. Journal of Proteome Research 2016;15:933–944 [PubMed: 26795031]
58. Johnson JL, Jackson CL. Atherosclerotic plaque rupture in the apolipoprotein e knockout mouse. Atherosclerosis 2001;154:399–406 [PubMed: 11166772]
59. Saarela J, Rehn M, Oikarinen A, Autio-Harmainen H, Pihlajaniemi T. The short and long forms of type xviii collagen show clear tissue specificities in their expression and location in basement membrane zones in humans. Am. J. Pathol 1998;153:611–626 [PubMed: 9708820]
60. Hotary KB, Allen ED, Brooks PC, Datta NS, Long MW, Weiss SJ. Membrane type i matrix metalloproteinase usurps tumor growth control imposed by the three-dimensional extracellular matrix. Cell 2003;114:33–45 [PubMed: 12859896]
61. Wolf K, Mazo I, Leung H, Engelke K, von Andrian UH, Deryugina EI, Strongin AY, Brocker EB, Friedl P. Compensation mechanism in tumor cell migration: Mesenchymal-amoeboid transition after blocking of pericellular proteolysis. J. Cell Biol 2003;160:267–277 [PubMed: 12527751]
62. Ogier C, Bernard A, Chollet AM, T LED, Hanessian S, Charton G, Khrestchatisky M, Rivera S. Matrix metalloproteinase-2 (mmp-2) regulates astrocyte motility in connection with the actin cytoskeleton and integrins. Glia 2006;54:272–284 [PubMed: 16845676]
63. von Nandelstadh P, Gucciardo E, Lohi J, Li R, Sugiyama N, Carpen O, Lehti K. Actin-associated protein palladin promotes tumor cell invasion by linking extracellular matrix degradation to cell cytoskeleton. Mol. Biol. Cell 2014;25:2556–2570 [PubMed: 24989798]
64. Mead TJ, Du Y, Nelson CM, Gueye NA, Drazba J, Dancevic CM, Vankemmelbeke M, Buttle DJ, Apte SS. Adamts9-regulated pericellular matrix dynamics governs focal adhesion-dependent smooth muscle differentiation. Cell Rep 2018;23:485–498 [PubMed: 29642006]
65. Frisch SM, Francis H. Disruption of epithelial cell-matrix interactions induces apoptosis. J. Cell Biol 1994;124:619–626 [PubMed: 8106557]
66. Chen YC, Bui AV, Diesch J, Manasseh R, Hausding C, Rivera J, Haviv I, Agrotis A, Htun NM, Jowett J, Hagemeyer CE, Hannan RD, Bobik A, Peter K. A novel mouse model of atherosclerotic plaque instability for drug testing and mechanistic/therapeutic discoveries using gene and microrna expression profiling. Circ. Res 2013;113:252–265 [PubMed: 23748430]
67. Van der Donckt C, Van Herck JL, Schrijvers DM, Vanhoutte G, Verhoye M, Blockx I, Van Der Linden A, Bauters D, Lijnen HR, Sluimer JC, Roth L, Van Hove CE, Fransen P, Knaapen MW, Hervent AS, De Keulenaer GW, Bult H, Martinet W, Herman AG, De Meyer GR. Elastin fragmentation in atherosclerotic mice leads to intraplaque neovascularization, plaque rupture, myocardial infarction, stroke, and sudden death. Eur. Heart J 2015;36:1049–1058 [PubMed: 24553721]
68. Schwartz SM, Galis ZS, Rosenfeld ME, Falk E. Plaque rupture in humans and mice. Arterioscler. Thromb. Vasc. Biol 2007;27:705–713 [PubMed: 17332493]
69. Jackson CL, Bennett MR, Biessen EA, Johnson JL, Krams R. Assessment of unstable atherosclerosis in mice. Arterioscler. Thromb. Vasc. Biol 2007;27:714–720 [PubMed: 17332492]
70. Falk E, Schwartz SM, Galis ZS, Rosenfeld ME. Putative murine models of plaque rupture. Arterioscler. Thromb. Vasc. Biol 2007;27:969–972 [PubMed: 17377150]

71. Jackson CL. Defining and defending murine models of plaque rupture. Arterioscler. Thromb. Vasc. Biol 2007;27:973–977 [PubMed: 17377151]
72. Schapira K, Heeneman S, Daemen MJ. Animal models to study plaque vulnerability. Curr. Pharm. Des 2007;13:1013–1020 [PubMed: 17430160]
73. Matoba T, Sato K, Egashira K. Mouse models of plaque rupture. Curr. Opin. Lipidol 2013;24:419–425 [PubMed: 23942269]
74. Silvestre-Roig C, de Winther MP, Weber C, Daemen MJ, Lutgens E, Soehnlein O. Atherosclerotic plaque destabilization: Mechanisms, models, and therapeutic strategies. Circ. Res 2014;114:214–226 [PubMed: 24385514]
75. Hellings WE, Peeters W, Moll FL, Pasterkamp G. From vulnerable plaque to vulnerable patient: The search for biomarkers of plaque destabilization. Trends Cardiovasc. Med 2007;17:162–171 [PubMed: 17574124]
76. Crea F, Libby P. Acute coronary syndromes: The way forward from mechanisms to precision treatment. Circulation 2017;136:1155–1166 [PubMed: 28923905]
77. Choy JC, Hung VH, Hunter AL, Cheung PK, Motyka B, Goping IS, Sawchuk T, Bleackley RC, Podor TJ, McManus BM, Granville DJ. Granzyme b induces smooth muscle cell apoptosis in the absence of perforin: Involvement of extracellular matrix degradation. Arterioscler. Thromb. Vasc. Biol 2004;24:2245–2250 [PubMed: 15472125]
78. Lindstedt KA, Kovanen PT. Proteolysis of pericellular matrix: A process linking inflammation to plaque destabilization and rupture. Arterioscler. Thromb. Vasc. Biol 2004;24:2205–2206 [PubMed: 15576642]
79. Michel JB. Anoikis in the cardiovascular system: Known and unknown extracellular mediators. Arterioscler. Thromb. Vasc. Biol 2003;23:2146–2154 [PubMed: 14551156]
80. Lupu F, Heim DA, Bachmann F, Hurni M, Kakkar VV, Kruithof EKO. Plasminogen activator expression in human atherosclerotic lesions. Arterioscler. Thromb. Vasc. Biol 1995;15:1444–1455 [PubMed: 7670960]
81. Kienast J, Padro T, Steins M, Li CX, Schmid KW, Hammel D, Scheld HH, van de Loo JC. Relation of urokinase-type plasminogen activator expression to presence and severity of atherosclerotic lesions in human coronary arteries. Thromb. Haemost 1998;79:579–586 [PubMed: 9531045]
82. Sayed S, Cockerill GW, Torsney E, Poston R, Thompson MM, Loftus IM. Elevated tissue expression of thrombomodulatory factors correlates with acute symptomatic carotid plaque phenotype. Eur. J. Vasc. Endovasc. Surg 2009;38:20–25 [PubMed: 19356953]
83. Svensson PA, Olson FJ, Hagg DA, Ryndel M, Wiklund O, Karlstrom L, Hulthe J, Carlsson LM, Fagerberg B. Urokinase-type plasminogen activator receptor is associated with macrophages and plaque rupture in symptomatic carotid atherosclerosis. Int. J. Mol. Med 2008;22:459–464 [PubMed: 18813852]
84. Gong Y, Fan Y, Hoover-Plow J. Plasminogen regulates stromal cell-derived factor-1/cxcr4-mediated hematopoietic stem cell mobilization by activation of matrix metalloproteinase-9. Arterioscler. Thromb. Vasc. Biol 2011;31:2035–2043 [PubMed: 21719761]
85. Lijnen HR. Plasmin and matrix metalloproteinases in vascular remodeling. Thromb. Haemost 2001;86:324–333 [PubMed: 11487021]
86. Meilhac O, Ho-Tin-Noe B, Houard X, Philippe M, Michel JB, Angles-Cano E. Pericellular plasmin induces smooth muscle cell anoikis. FASEB J 2003;17:1301–1303 [PubMed: 12738809]
87. Song J, Zhang X, Buscher K, Wang Y, Wang H, Di Russo J, Li L, Lutke-Enking S, Zarbock A, Stadtmann A, Striewski P, Wirth B, Kuzmanov I, Wiendl H, Schulte D, Vestweber D, Sorokin L. Endothelial basement membrane laminin 511 contributes to endothelial junctional tightness and thereby inhibits leukocyte transmigration. Cell Rep 2017;18:1256–1269 [PubMed: 28147279]
88. Graf J, Iwamoto Y, Sasaki M, Martin GR, Kleinman HK, Robey FA, Yamada Y. Identification of an amino acid sequence in laminin mediating cell attachment, chemotaxis, and receptor binding. Cell 1987;48:989–996 [PubMed: 2951015]
89. Celie JW, Rutjes NW, Keuning ED, Soininen R, Heljasvaara R, Pihlajaniemi T, Drager AM, Zweegman S, Kessler FL, Beelen RH, Florquin S, Aten J, van den Born J. Subendothelial heparan sulfate proteoglycans become major l-selectin and monocyte chemoattractant protein-1 ligands upon renal ischemia/reperfusion. Am. J. Pathol 2007;170:1865–1878 [PubMed: 17525255]

90. Senior RM, Gresham HD, Griffin GL, Brown EJ, Chung AE. Entactin stimulates neutrophil adhesion and chemotaxis through interactions between its arg-gly-asp (rgd) domain and the leukocyte response integrin. J. Clin. Invest 1992;90:2251–2257 [PubMed: 1469085]
91. Steffensen LB, Rasmussen LM. A role for collagen type iv in cardiovascular disease? Am J Physiol Heart Circ Physiol 2018;315:H610–H625 [PubMed: 29677463]
92. Yang W, Ng FL, Chan K, Pu X, Poston RN, Ren M, An W, Zhang R, Wu J, Yan S, Situ H, He X, Chen Y, Tan X, Xiao Q, Tucker AT, Caulfield MJ, Ye S. Coronary-heart-disease-associated genetic variant at the col4a1/col4a2 locus affects col4a1/col4a2 expression, vascular cell survival, atherosclerotic plaque stability and risk of myocardial infarction. PLoS Genet 2016;12:e1006127 [PubMed: 27389912]
93. Iyer D, Zhao Q, Wirka R, Naravane A, Nguyen T, Liu B, Nagao M, Cheng P, Miller CL, Kim JB, Pjanic M, Quertermous T. Coronary artery disease genes smad3 and tcf21 promote opposing interactive genetic programs that regulate smooth muscle cell differentiation and disease risk. PLoS Genet 2018;14:e1007681 [PubMed: 30307970]
94. Burleigh MC, Briggs AD, Lendon CL, Davies MJ, Born GV, Richardson PD. Collagen types i and iii, collagen content, gags and mechanical strength of human atherosclerotic plaque caps: Span-wise variations. Atherosclerosis 1992;96:71–81 [PubMed: 1418104]
95. Cheng GC, Loree HM, Kamm RD, Fishbein MC, Lee RT. Distribution of circumferential stress in ruptured and stable atherosclerotic lesions. A structural analysis with histopathological correlation. Circulation 1993;87:1179–1187 [PubMed: 8462145]
96. Katsuda S, Okada Y, Minamoto T, Oda Y, Matsui Y, Nakanishi I. Collagens in human atherosclerosis. Immunohistochemical analysis using collagen type-specific antibodies. Arterioscler. Thromb 1992;12:494–502 [PubMed: 1373075]
97. Redgrave JN, Lovett JK, Gallagher PJ, Rothwell PM. Histological assessment of 526 symptomatic carotid plaques in relation to the nature and timing of ischemic symptoms: The oxford plaque study. Circulation 2006;113:2320–2328 [PubMed: 16651471]
98. Mayranpaa MI, Heikkila HM, Lindstedt KA, Walls AF, Kovanen PT. Desquamation of human coronary artery endothelium by human mast cell proteases: Implications for plaque erosion. Coron. Artery Dis 2006;17:611–621 [PubMed: 17047445]
99. Fleg JL, Stone GW, Fayad ZA, Granada JF, Hatsukami TS, Kolodgie FD, Ohayon J, Pettigrew R, Sabatine MS, Tearney GJ, Waxman S, Domanski MJ, Srinivas PR, Narula J. Detection of high-risk atherosclerotic plaque: Report of the nhlbi working group on current status and future directions. JACC Cardiovasc Imaging 2012;5:941–955 [PubMed: 22974808]
100. Khan AA, Sikdar S, Hatsukami T, Cebral J, Jones M, Huston J, Howard G, Lal BK. Noninvasive characterization of carotid plaque strain. J. Vasc. Surg 2017;65:1653–1663 [PubMed: 28274754]

NOVELTY AND SIGNIFICANCE

What Is Known?

- Most myocardial infarctions and many strokes are caused by rupture of atherosclerotic arterial plaques.
- Candidate-gene approaches have associated elevated artery wall protease activity and proteolysis of plaque structural proteins—especially collagens—with plaque rupture in humans.
- Mouse models have established a causal relationship between elevated plaque protease activity and histologic features of plaque rupture.

What New Information Does This Article Contribute?

- Unbiased proteomic studies performed in a mouse model of protease-induced plaque rupture and in ruptured human plaques identify specific basement-membrane proteins that are depleted in both the mouse and human plaques.
- Bioinformatics analyses of the proteomics data identify extracellular proteolysis, loss of cell-substrate adhesion, inflammation, and apoptosis as key vascular wall processes that precede plaque rupture.
- Loss of plaque basement-membrane proteins predominates over loss of plaque collagens both in the mouse model and in ruptured human plaques.
- The mouse model of plaque rupture replicates biochemical processes—particularly those associated with extracellular matrix loss—that are found in ruptured human plaques.

Plaque rupture is the proximate cause of most atherosclerosis-associated morbidity and mortality (including most heart attacks and many strokes); however, the underlying molecular mechanisms are unknown. Identification of these mechanisms would guide development of therapeutics and might identify diagnostics that predict plaque rupture. Identification of plaque-rupture mechanisms would be facilitated by availability of an animal model that reproduced biochemical processes underlying plaque rupture, and in which vascular tissue was available before plaque rupture. Instead of using a candidate-gene approach, we used unbiased proteomics and bioinformatics to identify specific proteins and biochemical processes associated with plaque rupture. Moreover, we performed these studies both in ruptured human plaques and in a mouse model of protease-induced plaque rupture. We confirmed key findings in a human validation cohort. Extracellular proteolysis, loss of basement-membrane proteins, loss of cell-matrix adhesion, and inflammation, were common to both ruptured human plaques and the mouse model. Surprisingly, plaque collagens were minimally altered in both settings. Although specific proteolytic fragments were not identified, combined data from the mouse and human studies illuminated a series of biochemical processes through which elevated plaque protease activity leads to basement-membrane proteolysis, apoptosis, inflammation, and plaque rupture. These findings suggest novel and attractive targets for interventions aimed at preventing plaque rupture.

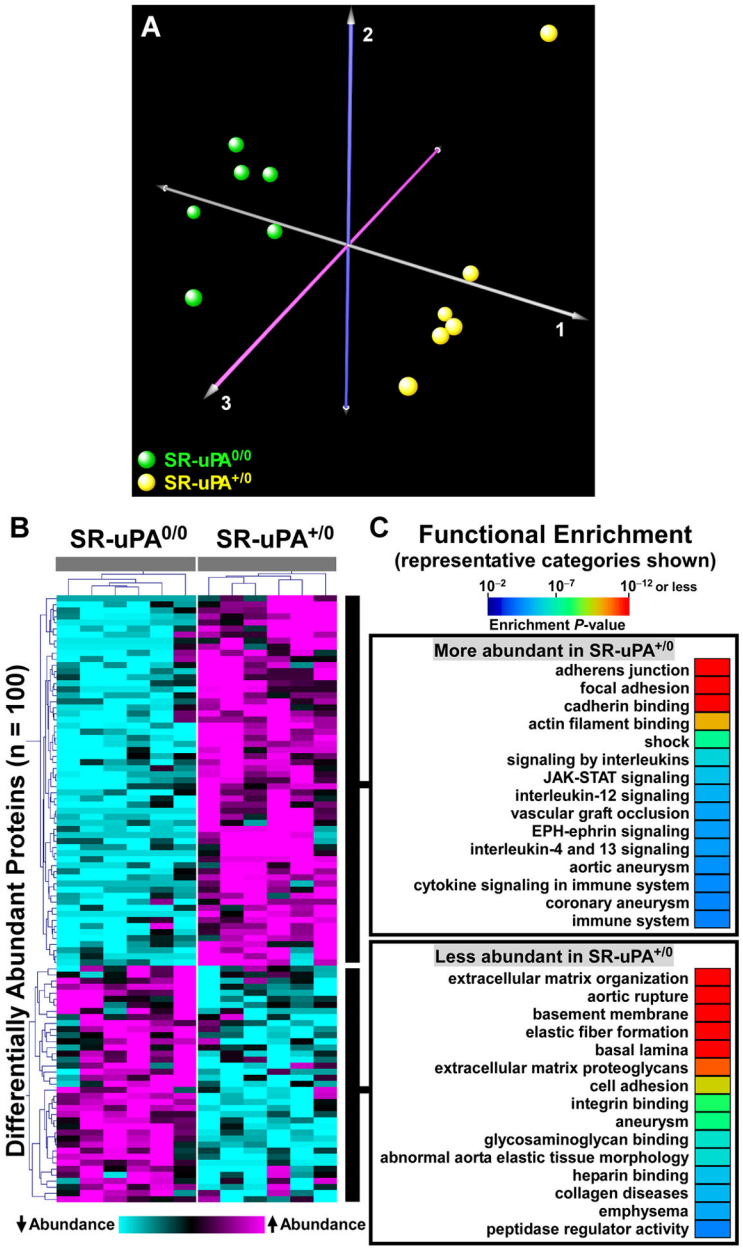

Figure 1. Proteomic analyses identify global differences in protein abundance and biological processes in aortas of SR-uPA$^{+/0}$ and SR-uPA$^{0/0}$ mice.

(**A**) Correspondence analysis was applied to 775 proteins identified in extracts of aortas of SR-uPA$^{+/0}$ and SR-uPA$^{0/0}$ mice. Individual mice of the 2 genotypes are represented by colored spheres. (**B**) Heatmap of two-dimensional hierarchical cluster analysis for the 100 differentially abundant proteins (FDR < 0.05). A complete list of these proteins is in Online Data Set II. (**C**) Functional enrichment analysis of the differentially abundant proteins reveals over-represented biological processes. A complete list of these categories is in Online Data Sets III and IV.

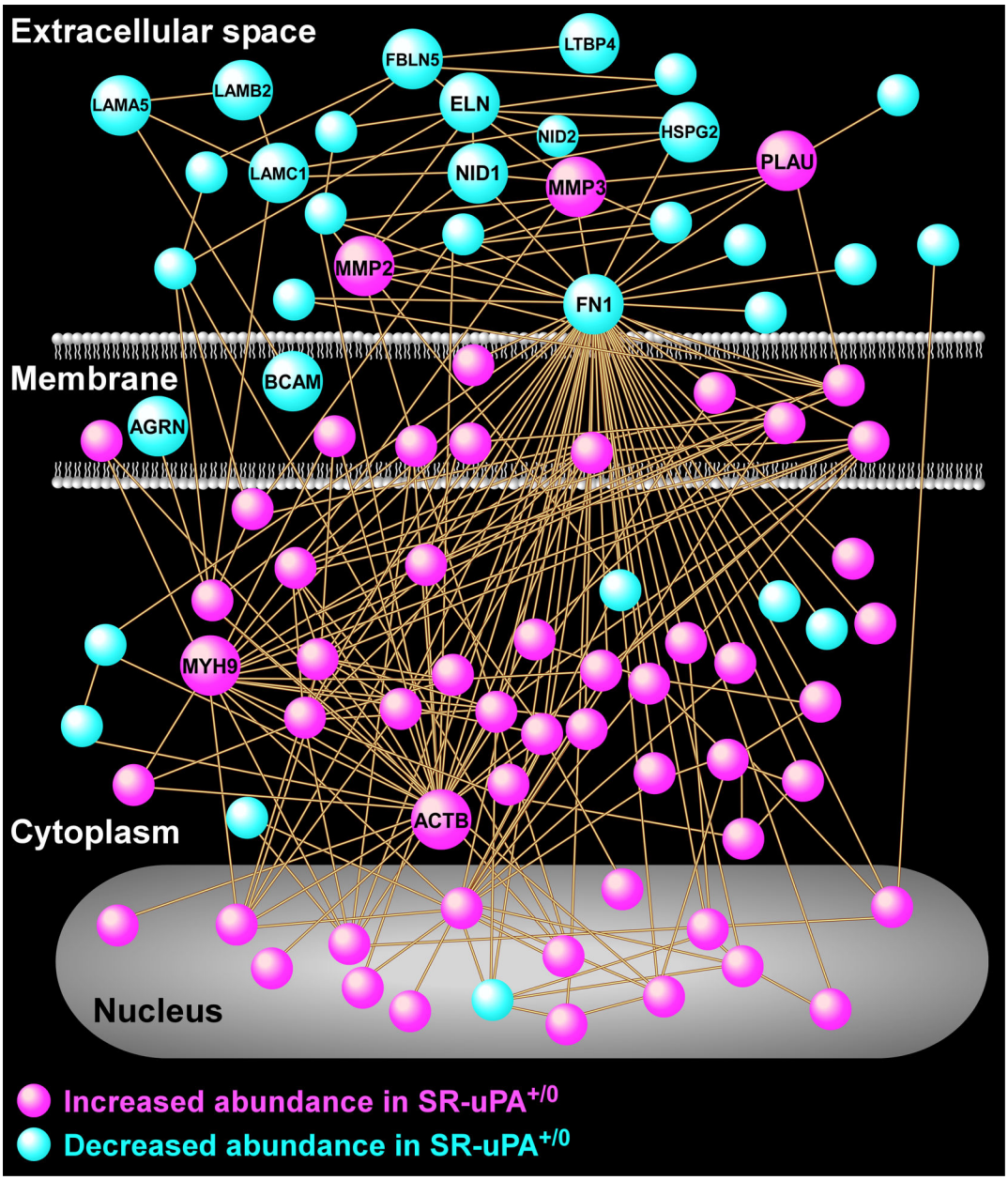

Figure 2. Protein-interaction network analysis reveals numerous interactions of proteins that are differentially abundant in aortas of SR-uPA$^{+/0}$ mice.

A protein-protein relational network was built based on experimentally validated direct interactions. The network is comprised of 87 proteins, each portrayed as a circular node (all nodes are identified in Online Data Set V). Key highly connected nodes (hubs) are labeled together with 2 members of the matrix metalloproteinase family of extracellular proteases, and several extracellular matrix components.

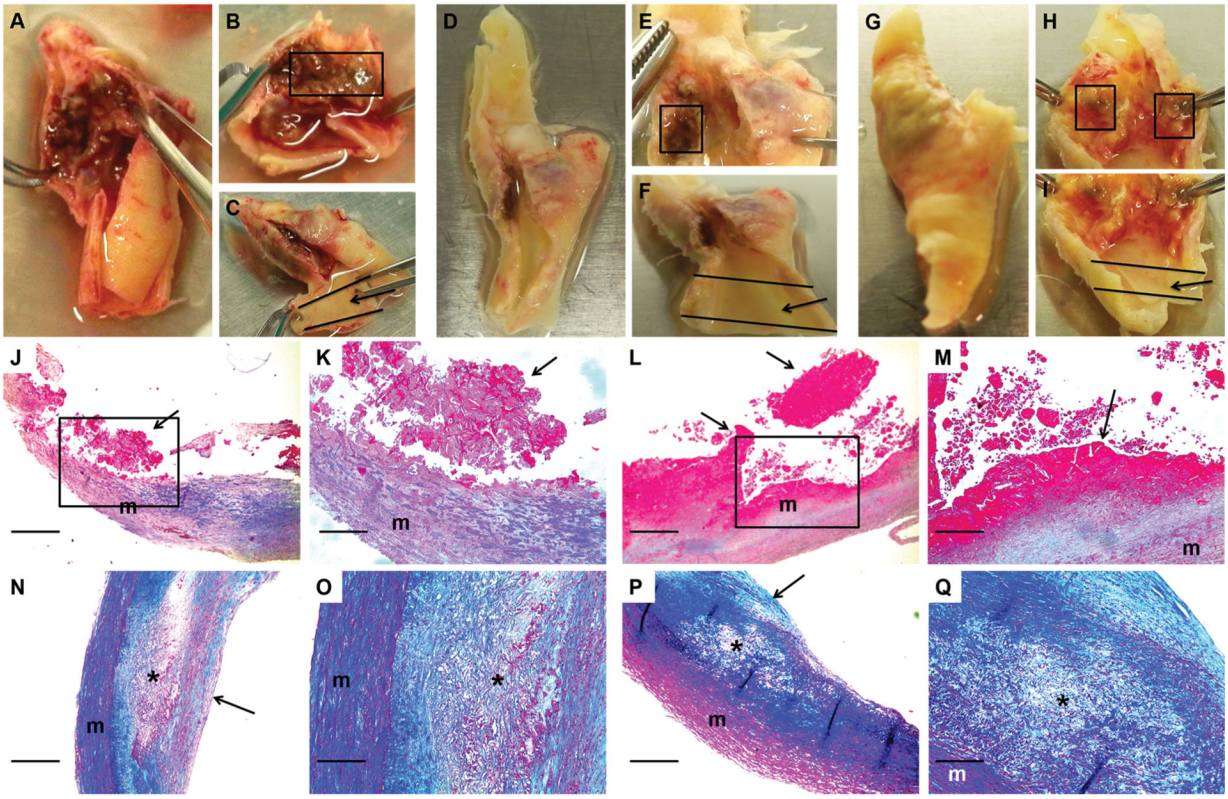

Figure 3. Macroscopic and histologic images of ruptured and stable segments of human carotid plaques.

Human carotid plaques were removed for clinical indications. Images are of 3 freshly harvested plaques (**A-C**, **D-F**, and **G-I**) and stained sections of 2 ruptured (**J-K** and **L-M**) and 2 stable (**N-O** and **P-Q**) plaques. Ruptured segments (boxes in **B**, **E**, and **H**) and stable segments (arrows in **C**, **F**, and **I**) were dissected free. A scalpel was used to cut thin slices from the caudal and cranial edges of the dissected segments. These slices were embedded in paraffin, and the remainder of each segment was used for protein extraction. Sections of 2 ruptured plaque segments (**J-M;** boxes in **J** and **L** are expanded in **K** and **M**) show disrupted intima with adherent thrombus (arrows; thrombus fragmentation is likely sectioning artifact). Sections of 2 stable plaque segments (**N-O** and **P-Q**; **O** and **Q** are expanded from **N** and **P**, respectively) show intact fibrous caps (arrows in **N** and **P**) and lipid-rich necrotic cores (asterisks) containing cholesterol clefts and foam cells. **J-Q**, m = vascular media. Size bars are 50 μm (**J**, **L**, **N**, and **P**) and 20 μm (**K**, **M**, **O**, and **Q**). **J-Q**, Masson's trichrome stain.

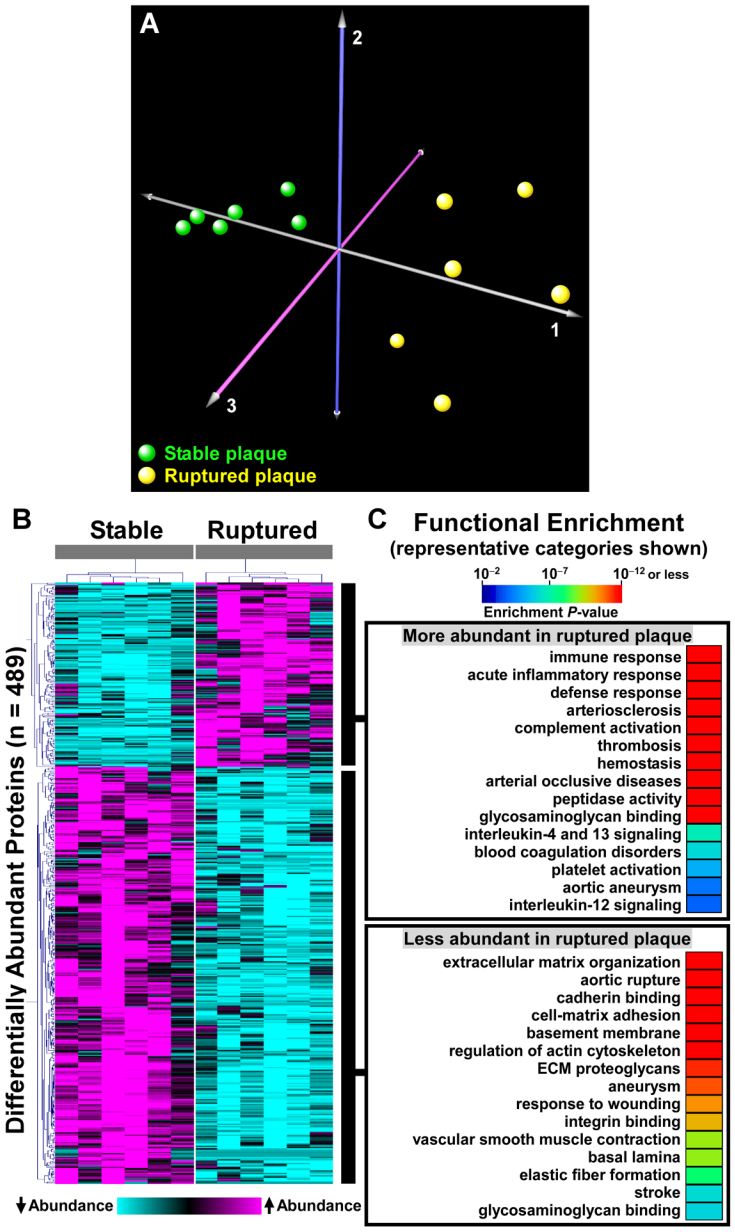

Figure 4. Proteomic analyses identify global differences in protein abundance and biological processes in paired samples of ruptured and stable human carotid artery plaque segments.

(**A**) Correspondence analysis was applied to the 1,161 identified proteins. Individual plaques from the 2 areas are represented by colored spheres. (**B**) Heatmap of two-dimensional hierarchical cluster analysis for the 489 proteins that are differentially abundant (FDR <0.05) between ruptured and stable plaque segments. A complete list of these proteins is in Online Data Set XII (**C**) Functional enrichment analysis of the differentially abundant proteins reveals over-represented biological processes. A complete list is in Online Data Sets XIII and XIV.

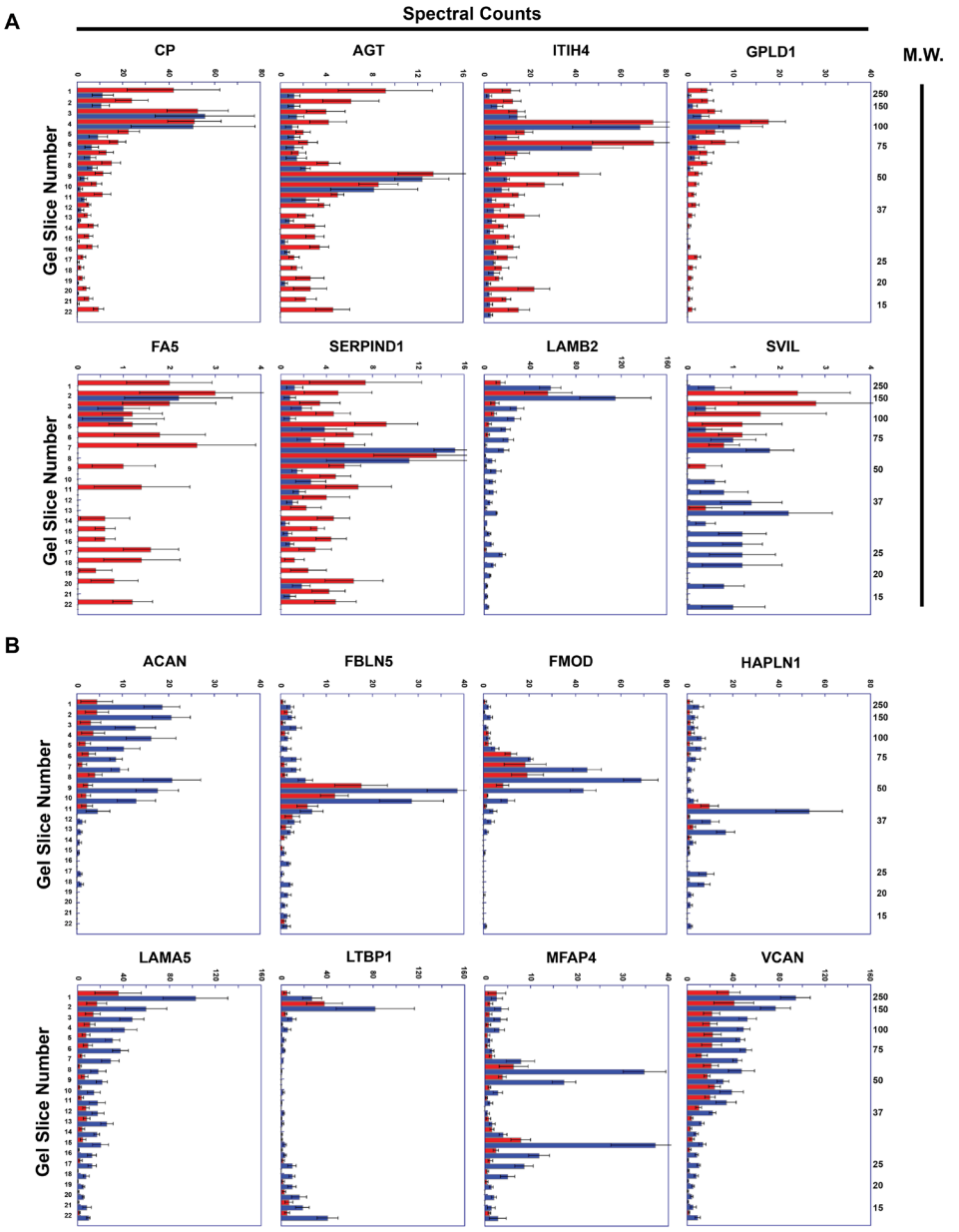

Figure 5. Representative peptographs of extracts of ruptured vs. stable human plaque segments.

(**A** and **B**) Extracts of ruptured (red) and adjacent stable (blue) segments of 5 human carotid plaques were analyzed using the PROTOMAP protocol. The extracts were subjected to SDS-PAGE and the gels were cut into 22 slices, each corresponding to a molecular-weight range. After in-gel trypsin digestion, peptides were extracted, identified by tandem mass spectrometry, and spectral counts were aggregated over all 22 slices. (**A**) Proteins with differential abundance of lower-molecular-weight peptides in extracts of ruptured vs. stable segments: ceruloplasmin (CP), angiotensinogen (AGT), inter-alpha-trypsin inhibitor heavy chain (ITIH4), phosphatidylinositol-glycan-specific phospholipase D (GPLD1), coagulation factor V (FA5), heparin cofactor 2 (SERPIND1), laminin subunit beta-2 (LAMB2), and supervillin (SVIL). (**B**) ECM proteins that are significantly less abundant in extracts of

ruptured vs. stable human plaque segments: aggrecan core protein (ACAN), fibulin-5 (FBLN5), fibromodulin (FMOD), hyaluronan and proteoglycan link protein 1 (HAPLN1), laminin subunit alpha-5 (LAMA5), microfibril-associated glycoprotein 4 (MFAP4), latent-transforming growth factor beta-binding protein 1, and versican (VCAN). (**A** and **B**) Horizontal bars in each peptograph portray the total spectral counts for protein-specific peptides in each of the 22 gel slices (mean ± SEM; n = 5). Gel-slice number is on the leftward y-axis; molecular weight of the gel slices (in kiloDaltons) is on the rightward y-axis.

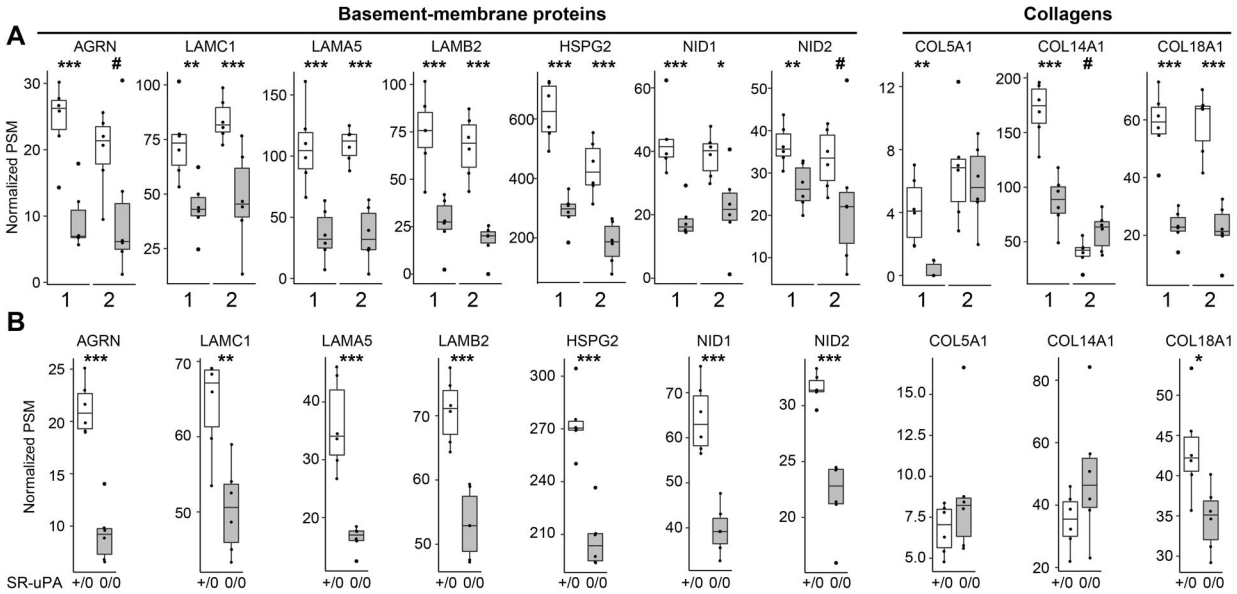

Figure 6. Depletion of basement-membrane proteins in ruptured human carotid plaques and in aortas of SR-uPA$^{+/0}$ mice.

(**A**) Data from 2 sets of human carotid plaques. Shotgun proteomics was performed on stable (open bars) and ruptured (shaded bars) segments of two independent sets of plaques (1 and 2). Analyses were performed independently, 1 year apart. Proteins were selected for this analysis based on their significantly decreased abundance in the first set of human plaques and—for basement-membrane proteins—congruently decreased abundance in SR-uPA$^{+/0}$ mouse aortas. (**B**) Data from aortas of 20-week-old SR-uPA$^{+/0}$ and SR-uPA$^{0/0}$ mice. (**A** and **B**) Individual data points (n=6 per group) indicate individual plaque segments (**A**) or aortas (**B**); group medians and interquartile ranges are shown. PSM= peptide-spectrum match. *P* values: #<0.1, *<0.05, **<0.01 ***<0.005.

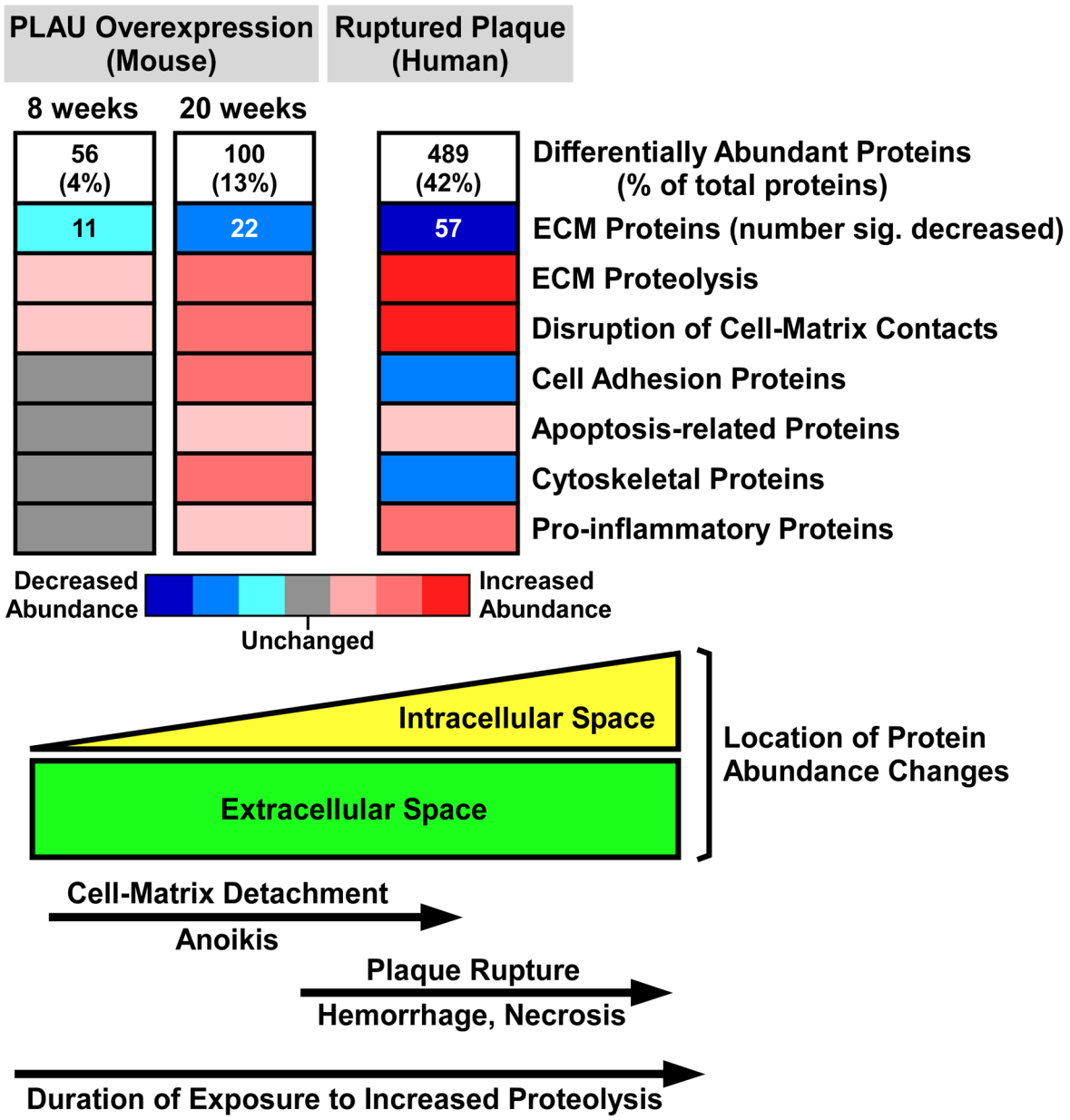

Figure 7. Shotgun proteomic analyses of mouse and human plaques suggest molecular and cellular mechanisms that connect extracellular proteolysis with plaque rupture.

Proteomic data from the mouse model of PLAU overexpression (2 time points) and from human plaques show stepwise increases in the number of differentially abundant proteins (Online Data Sets II, IX, and XII), and corresponding decreases in ECM protein abundance (Online Data Sets IV, XI, and XIV). Decreased ECM protein abundance is likely caused by increased proteolysis. Eight weeks exposure to elevated PLAU activity initiates disruption of cell-matrix contacts, which increases by 20 weeks. Also by 20 weeks, ECM protein loss stimulates homeostatic increases in cell-adhesion and cytoskeletal proteins, inflammation, as well as programmed cell death (anoikis) triggered by loss of cell-matrix contacts. Advanced human plaques have more extensive proteolysis and disruption of cell-matrix contacts, causing anoikis and cell necrosis with attendant loss of cell-adhesion and cytoskeletal

proteins. Plaque-cell death weakens plaque structure, leading to rupture and an inflammatory response to tissue injury. The lower part of the figure illustrates the predominance of extracellular protein abundance changes at early stages of plaque proteolysis and the shift towards intracellular protein abundance changes at later stages.

Table 1.

Cytoskeletal, Cell Adhesion, and Extracellular Matrix Proteins with Significantly Different Abundance in Aortas of SR-uPA$^{+/0}$ Mice

Cytoskeletal Proteins* Increased in SR-uPA$^{+/0}$ aortas			**Cell Adhesion Proteins† Increased in SR-uPA$^{+/0}$ aortas**			**Extracellular Matrix Proteins‡ Decreased in SR-uPA$^{+/0}$ aortas**		
Protein	SR-uPA$^{+/0}$	SR-uPA$^{0/0}$	Protein	SR-uPA$^{+/0}$	SRuPA$^{0/0}$	Protein	SR-uPA$^{+/0}$	SR-uPA$^{0/0}$
ARPC1B	7.4 ± 2.5	1.6 ± 0.6	HDLBP	9 ± 3.3	1.9 ± 1.4	EMILIN1	3.2 ± 1.7	11.5 ± 2.9
CAPZB	11 ± 2.5	5.8 ± 1.7	ACTB	57.1 ± 6.8	42.9 ± 8	LTBP4	17.9 ± 5	40.4 ± 4.3
CFL1	15.8 ± 2.7	9.9 ± 1.2	ARPC1B	7.4 ± 2.5	1.6 ± 0.6	AGRN	9.3 ± 2.7	21.3 ± 2.4
MYH9	42.6 ± 10.1	22.7 ± 5.6	CAPZB	11 ± 2.5	5.8 ± 1.7	ATP5B	70.4 ± 8.1	95.9 ± 13
LCP1	10.3 ± 1.1	6.2 ± 2.2	CFL1	15.8 ± 2.7	9.9 ± 1.2	COL15A1	18.3 ± 5.1	29.8 ± 5.8
SPTBN1	14.4 ± 4.5	4.1 ± 1.6	EEF2	18 ± 2.2	10.7 ± 3.7	COL1A2	12.2 ± 3.5	18.2 ± 2.9
CORO1C	3.9 ± 1.1	1.5 ± 1.3	GNB2	9.5 ± 1.8	4.3 ± 0.3	ELN	8.7 ± 2.9	15 ± 2.5
FLNB	9.3 ± 1.1	2.1 ± 1.4	PDIA3	46.5 ± 4.5	36.6 ± 4.7	FN1	309.3 ± 35.9	399.7 ± 40.9
SEPT9	3 ± 0.9	0.5 ± 0.8	RPS2	10.3 ± 1.6	6.2 ± 1.2	HSPG2	207.4 ± 16.3	272.8 ± 17.5
ACTN4	28.7 ± 2.3	14.5 ± 2.4	ANXA1	28.9 ± 3.4	22.2 ± 3.1	LAMA5	16.4 ± 2.2	35.8 ± 7.8
AHNAK	54.2 ± 9.7	36.2 ± 6.7	LRP1	16.2 ± 3.4	7.8 ± 0.4	LAMB2	53.2 ± 5.3	70.7 ± 5
ACTB	57.1 ± 6.8	42.9 ± 8	MYH9	42.6 ± 10.1	22.7 ± 5.6	LOXL1	38.9 ± 3.2	58.9 ± 8.4
MAP4	4.7 ± 3	0.4 ± 0.6	PLAU	17.4 ± 6.5	0 ± 0	NID1	39.6 ± 5.3	64.3 ± 7.7
PLEC	25.8 ± 2.3	7.8 ± 2.2	PLEC	25.8 ± 2.3	7.8 ± 2.2	NID2	21.9 ± 3.3	31.5 ± 1.3
TCP1	15.1 ± 1.9	8.2 ± 2.7	LCP1	10.3 ± 1.1	6.2 ± 2.2	EFEMP1	2.5 ± 1.2	11.8 ± 4.1
MVP	21.5 ± 3.4	12.2 ± 3.2	RPS5	4.3 ± 1.3	1.9 ± 0.7	SERPINE2	8.9 ± 3	16.9 ± 2.2
RCC1	4.1 ± 1	1.8 ± 1.4	SPTBN1	14.4 ± 4.5	4.1 ± 1.6	VTN	17.9 ± 4.2	25.3 ± 3.9
ANXA1	28.9 ± 3.4	22.2 ± 3.1	THY1	2.8 ± 0.6	0.7 ± 0.9	WISP2	6.4 ± 2.3	10.8 ± 2
THY1	2.8 ± 0.6	0.7 ± 0.9	HSP90B1	41.6 ± 2.6	24.7 ± 5.3	FBLN5	46.5 ± 5.6	80.1 ± 10.5
HSP90B1	41.6 ± 2.6	24.7 ± 5.3	CORO1C	3.9 ± 1.1	1.5 ± 1.3	POSTN	51.4 ± 5.3	63.2 ± 3.7
ANXA8	8.5 ± 2.3	3.7 ± 1.2	FLNB	9.3 ± 1.1	2.1 ± 1.4	HTRA1	13.5 ± 6.7	29.8 ± 2.5
EEF2	18 ± 2.2	10.7 ± 3.7	SEPT9	3 ± 0.9	0.5 ± 0.8	MFAP4	36 ± 5.9	47.4 ± 6
GNB1	13.4 ± 2.2	3.9 ± 1.1	SND1	10.1 ± 5.4	2.8 ± 1.2	PLG	10.3 ± 6.6	22.2 ± 5.6
VCP	31.3 ± 5.8	19 ± 4	ACTN4	28.7 ± 2.3	14.5 ± 2.4	BCAM	5.5 ± 3.5	12 ± 3.1
			AHNAK	54.2 ± 9.7	36.2 ± 6.7	LAMC1	50.5 ± 5.9	64.2 ± 6.4
			RPL4	16.7 ± 2.1	11.5 ± 2.5			
			PUF60	5.8 ± 1.2	3 ± 1.2			
			DDOST	10.9 ± 3	5.5 ± 2			

Data are mean ± SD. All differences were significant (FDR< 0.05; Online Data Set II)

*Includes all proteins in GO categories: 0015629 (actin cytoskeleton), 0030863 (cortical cytoskeleton), 0005856 (cytoskeleton), 0007010 (cytoskeleton organization), or 0008092 (cytoskeletal protein binding).

†Includes all proteins in GO categories: 005912 (adherens junction), 005925 (focal adhesion), or 0007155 (cell adhesion).

‡Includes all proteins in GO categories: 0031012 (extracellular matrix), 00030198 (extracellular matrix organization), 0050840 (extracellular matrix binding), 0005201 (extracellular matrix structural constituent, or 0005604 (basement membrane; these are in bold type).

Table 2.

GO categories significantly* overrepresented by less-abundant proteins in both SR-uPA$^{+/0}$ aortas and ruptured segments of human plaques.

Cellular Component	Biological Process	Molecular Function
Proteinaceous extracellular matrix	Extracellular structure organization	Cell adhesion molecule binding
Extracellular matrix	Extracellular matrix organization	Integrin binding
Extracellular matrix component	Regulation of cell-substrate adhesion	Extracellular matrix structural constituent
Basement membrane	Biological adhesion	Extracellular matrix binding
Basal lamina	Cell-substrate adhesion	Glycosaminoglycan binding
Laminin complex	Cell adhesion	
	Cell-matrix adhesion	
	Regulation of cell adhesion	

* For all categories, FDR < 0.01 in both mouse aortas and human plaques.